© 2022. Published by The Company of Biologists Ltd | Journal of Cell Science (2022) 135, jcs259396. doi:10.1242/jcs.259396

RESEARCH ARTICLE

The retromer complex regulates *C. elegans* development and mammalian ciliogenesis

Shuwei Xie[1], Carter Dierlam[2], Ellie Smith[2], Ramon Duran[2], Allana Williams[2], Angelina Davis[3,*], Danita Mathew[2,*], Naava Naslavsky[1], Jyoti Iyer[2,‡] and Steve Caplan[1,4,‡]

ABSTRACT

The mammalian retromer consists of subunits VPS26 (either VPS26A or VPS26B), VPS29 and VPS35, and a loosely associated sorting nexin (SNX) heterodimer or a variety of other SNX proteins. Despite involvement in yeast and mammalian cell trafficking, the role of retromer in development is poorly understood, and its impact on primary ciliogenesis remains unknown. Using CRISPR/Cas9 editing, we demonstrate that *vps-26*-knockout worms have reduced brood sizes, impaired vulval development and decreased body length, all of which have been linked to ciliogenesis defects. Although preliminary studies did not identify worm ciliary defects, and impaired development limited additional ciliogenesis studies, we turned to mammalian cells to investigate the role of retromer in ciliogenesis. VPS35 localized to the primary cilium of mammalian cells, and depletion of VPS26, VPS35, VPS29, SNX1, SNX2, SNX5 or SNX27 led to decreased ciliogenesis. Retromer also coimmunoprecipitated with the centriolar protein, CP110 (also known as CCP110), and was required for its removal from the mother centriole. Herein, we characterize new roles for retromer in *C. elegans* development and in the regulation of ciliogenesis in mammalian cells, suggesting a novel role for retromer in CP110 removal from the mother centriole.

KEY WORDS: Centrosome, Ciliogenesis, CP110, Retromer, VPS26, VPS35, VPS29, SNX1, SNX2, SNX5, SNX27

INTRODUCTION

Retromer is a conserved protein complex involved in the sorting and trafficking of endosomal cargo (Naslavsky and Caplan, 2018; Wang et al., 2018). Based on initial findings in yeast (Seaman et al., 1998), the mammalian retromer has been described as a 'core complex' of the VPS26–VPS29–VPS35 trimer [note there are two VPS26 isoforms evolved from duplicated genes, VPS26A and VPS26B; (Bugarcic et al., 2011; Kerr et al., 2005)] (Haft et al., 2000). This core complex binds to a heterodimeric sorting nexin duo comprising either SNX1 or SNX2 (Griffin et al., 2005; Rojas et al., 2007) with either SNX5 or SNX6 (Cullen and Korswagen, 2012; Haft et al., 2000), but can also interact with other SNX proteins (McNally and Cullen, 2018). However, evidence in mammals suggests that the SNX protein association with the retromer core is less stable than in yeast (Harbour et al., 2010) and that the SNX dimers can function independently of the core complex (Evans et al., 2020; Kvainickas et al., 2017; Simonetti et al., 2019). Although the sorting nexin proteins bind to endosomal-enriched phosphatidylinositol-3-phosphate via their phox domains (Seaman and Williams, 2002), the original function identified for the retromer core complex proteins was in binding to select cargo receptors and the regulation of their sorting/trafficking (Arighi et al., 2004; Seaman, 2004). Newer studies support the notion that sorting nexins, including the more peripherally associated SNX27, SNX17 and SNX3 proteins, also interact with cargo receptors and play an important role in the cargo selection process (Clairfeuille et al., 2016; Farfán et al., 2013; Harterink et al., 2011; Kovtun et al., 2018; Lauffer et al., 2010; Leneva et al., 2021; Lucas et al., 2016; Seaman, 2021; Steinberg et al., 2013; Steinberg et al., 2012; Strochlic et al., 2007; Temkin et al., 2011; van Kerkhof et al., 2005). Retromer was originally described for its role in endosomal retrieval of the carboxypeptidase Y (CPY) hydrolase receptor, Vps10p, back to the Golgi after it delivers CPY to the yeast vacuole (Seaman et al., 1997), as well as its function in the retrieval of the cation-independent mannose-6-phosphate receptor from endosomes to the Golgi in mammalian cells (Arighi et al., 2004). However, recent studies indicate that retromer plays a central role in many additional cellular trafficking events (Seaman, 2021; Wang et al., 2018).

The retromer complex has been documented as having a wide and growing array of functions in recent years. In addition to membrane trafficking and the regulation of mannose-6-phosphate receptor recovery from endosomes to the Golgi (Arighi et al., 2004; Reddy and Seaman, 2001; Seaman, 2004), and its role in receptor recycling, endosomal tubule dynamics and modulation of the actin cytoskeleton through FAM21 and the WASH complex (Gokool et al., 2007; Gomez and Billadeau, 2009; Harbour et al., 2010; Strochlic et al., 2007), retromer has also been implicated in apoptosis (Farmer et al., 2019), mitochondrial membrane dynamics and Parkinson's disease (Braschi et al., 2010; Farmer et al., 2018; Farmer et al., 2017; Kumar et al., 2012; Vilariño-Güell et al., 2011; Wang et al., 2017; Zimprich et al., 2011), as well as in the regulation of centrosome duplication (Xie et al., 2018).

The retromer core complex of VPS26–VPS29–VPS35, whose structure has recently been elucidated (Chen et al., 2019; Norwood et al., 2011), is highly conserved throughout the evolutionary ladder from yeast, to invertebrates such as *C. elegans*, as well as in humans (Wang et al., 2018). For example, there is 58% identity shared between human VPS26A and the *C. elegans* VPS-26 proteins, 58% identity shared between human VPS29 and the *C. elegans* VPS-29 proteins, and 49% identity between the human VPS35 and the worm

[1]Department of Biochemistry & Molecular Biology, University of Nebraska Medical Center, Omaha, NE 68198, USA. [2]Department of Chemistry and Biochemistry, University of Tulsa, Tulsa, OK 74104, USA. [3]School of Science and Mathematics, Tulsa Community College, Tulsa, OK 74115, USA. [4]Fred and Pamela Buffett Cancer Center, University of Nebraska Medical Center, Omaha, NE 68198, USA.
*These authors contributed equally to this work

‡Authors for correspondence (jgi2708@utulsa.edu; scaplan@unmc.edu)

A.W., 0000-0001-7048-9524; J.I., 0000-0002-0942-6919; S.C., 0000-0001-9445-4297

Handling Editor: Jennifer Lippincott-Schwartz
Received 24 September 2021; Accepted 11 April 2022

Journal of Cell Science (2022) 135, jcs259396. doi:10.1242/jcs.259396

VPS-35 proteins. Whereas the role of the retromer complex has been studied extensively in yeast and in mammalian systems, the function of retromer and its role in development in invertebrates, such as *C. elegans*, is incompletely understood. It has been observed that worms with mutant *vps-29* or *vps-35* genes display impaired trafficking of the receptor-type guanylate cyclase GCY-9, which accumulates in BAG chemosensory neurons (Coudreuse et al., 2006; Martinez-Velazquez and Ringstad, 2018). Recent studies have shown a role for worm retromer subunits in anteroposterior polarity, Wnt signaling and Q cell migration (Prasad and Clark, 2006). Furthermore, *vps-35*-knockout worms have reduced mTorc1 signaling and increased lifespans (Kvainickas et al., 2019). In addition, a variety of other functions have been attributed to retromer in *C. elegans* including bone morphogenic signaling (Gleason et al., 2014, 2017), CED-1 receptor recycling (Chen et al., 2010), glutamate receptor recycling (Zhang et al., 2012a), and retrograde recycling of iron transporters (Patel et al., 2018). Nonetheless, important questions remain with regard to the role of retromer in the *C. elegans* nematode model system, particularly with regard to development. Moreover, despite the interaction of retromer with EHD proteins and their binding partner (Gokool et al., 2007; McKenzie et al., 2012; Zhang et al., 2012b), MICAL-L1 (Zhang et al., 2012c), and the known involvement of the latter proteins in regulating primary ciliogenesis (Lu et al., 2015; Xie et al., 2019), to date the involvement of retromer proteins in primary cilia biogenesis remains to be elucidated.

Herein, we used CRISPR-based technology to first obtain a *vps-26::ha* tagged *C. elegans* strain to detect endogenous VPS-26 expression in worms. Using this strain as a background, we again used CRISPR to successfully knockout VPS-26 expression. We demonstrate that although *vps-26* homozygous knockout worms are no less viable than their wild-type counterparts, the knockout worms have dramatically reduced brood sizes, typically with 10-fold fewer progeny. Impaired vulval development was observed in the *vps-26*-knockout worms, which could explain why these worms produce fewer progeny. In addition to decreased brood sizes, the *vps-26*-knockout adult worms also display a significant decrease in body length, a characteristic previously linked to defects in primary ciliogenesis (Fujiwara et al., 2002). Analysis of ciliogenesis in *C. elegans* phasmid cilia did not reveal differences in ciliary length in *vps-26*-knockout worms. However, some ciliary mutants do not exhibit significant differences in ciliary length despite possessing other ciliary defects, such as transition zone defects (Schouteden et al., 2015). Therefore, it is presently unclear whether *vps-26*-knockout worms have ciliogenesis defects. Owing to the severe vulval defects and low brood sizes of *vps-26*-knockout worms, further experiments to investigate the role of retromer in ciliogenesis in worms were not feasible. Hence, we elected to assess the role of retromer subunits in primary ciliogenesis in RPE-1 cells. siRNA-based knockdown of VPS26A (hereafter referred to as VPS26), VPS35 and VPS29, or the SNX1, SNX2, SNX5 and SNX27 sorting nexins led to reduced levels of primary ciliogenesis in RPE-1 cells. Despite retromer interaction with EHD proteins and MICAL-L1, the retromer subunits were not required for the localization of either MICAL-L1 or EHD1 to primary cilia. Conversely, the retromer subunit VPS35 was recruited to primary cilia independently of MICAL-L1 and EHD1. Finally, we demonstrate that depletion of either VPS26 or VPS35 leads to the failure of CP110 removal from the mother centriole, which is a key step in primary ciliogenesis. Moreover, we provide initial evidence of a complex formed between CP110 (also known as CCP110) and the retromer subunits, hinting at a potential explanation for the elusive mechanism of CP110 removal from the mother centriole as ciliogenesis progresses. Overall, our study highlights new roles for the retromer complex in *C. elegans* development and in the regulation of mammalian ciliogenesis, expanding on the broad function of retromer and providing new clues to the mechanism of CP110 removal from the mother centriole.

RESULTS

Generation of CRISPR/Cas9 gene-edited *vps-26* worm strains

To investigate the role of the retromer complex in *C. elegans*, we probed the function of the conserved retromer complex subunit VPS-26, which shares 58% identity with the human VPS26A subunit. Indeed, it has been demonstrated that knockdown of VPS26 expression in mammalian cells leads to destabilization of VPS35, thus disrupting the entire retromer complex (Seaman, 2004). The lack of an available antibody to the *C. elegans* VPS-26 protein led us to generate a worm strain expressing epitope-tagged VPS-26. To study the expression and localization of *C. elegans* VPS-26, CRISPR/Cas9 genome editing was performed to create a strain expressing VPS-26 fused to a C-terminal hemagglutinin (HA) tag. The schematic of the repair template and the generated *vps-26::ha* strain is shown in Fig. 1A. To facilitate screening of positively edited worms, a NdeI restriction site was introduced into the repair template (Fig. 1A). Positive F1 heterozygotes were first identified by PCR and restriction digestion followed by agarose gel electrophoresis. Subsequently, we again screened the progeny of the positively edited heterozygous worms for homozygosity of the edit (Fig. 1B). As shown in Fig. 1B, homozygous-edited *vps-26::ha* worms could be successfully identified. The identified homozygotes were further confirmed by DNA sequencing (Fig. 1C).

Once the *vps-26::ha* homozygotes were confirmed, immunoblotting was performed, and we detected abundant VPS-26::HA protein expression in *C. elegans* whole-worm lysates (Fig. 1D). We then immunostained early embryos expressing VPS-26::HA to characterize the localization pattern of endogenously expressed VPS-26 (Fig. 1E,F). Accordingly, immunofluorescence analysis demonstrated that VPS-26::HA exhibits a punctate localization pattern around the spindle microtubules in one-cell and two-cell stage *C. elegans* embryos in mitosis (Fig. 1E,F).

To study the function of the retromer complex in *C. elegans*, CRISPR/Cas9 genome editing was used to knockout VPS-26 protein expression (Fig. 2). Specifically, two premature stop codons separated by a single base were introduced into the CRISPR repair template to cause a frameshift mutation (Fig. 2A). The schematic for the CRISPR repair template used to knockout VPS-26 expression is shown in Fig. 2A. The *vps-26::ha* strain characterized in Fig. 1 was used as the background strain to knockout VPS-26 expression. Upon identifying homozygous-edited worms, DNA sequencing was performed to confirm successful integration of the CRISPR edit into the *vps-26* gene (Fig. 2B,C). Alignment of the sequencing data with the wild-type *vps-26* gene sequence demonstrated that a part of the *vps-26* gene sequence was deleted and two premature stop codons and the frameshift mutation were successfully inserted at the 5′ end of the *vps-26* gene sequence (Fig. 2B). Immunoblot analysis of whole worm lysates showed that VPS-26::HA expression was undetectable in the *vps-26*-knockout strain as compared with the control *vps-26::ha* strain (Fig. 2D). This *vps-26*-knockout strain was named *vps-26*(*luv21*). For the sake of simplicity, the *vps-26*(*luv21*) strain has been referred to as the *vps-26*-knockout strain throughout this manuscript.

Journal of Cell Science (2022) 135, jcs259396. doi:10.1242/jcs.259396

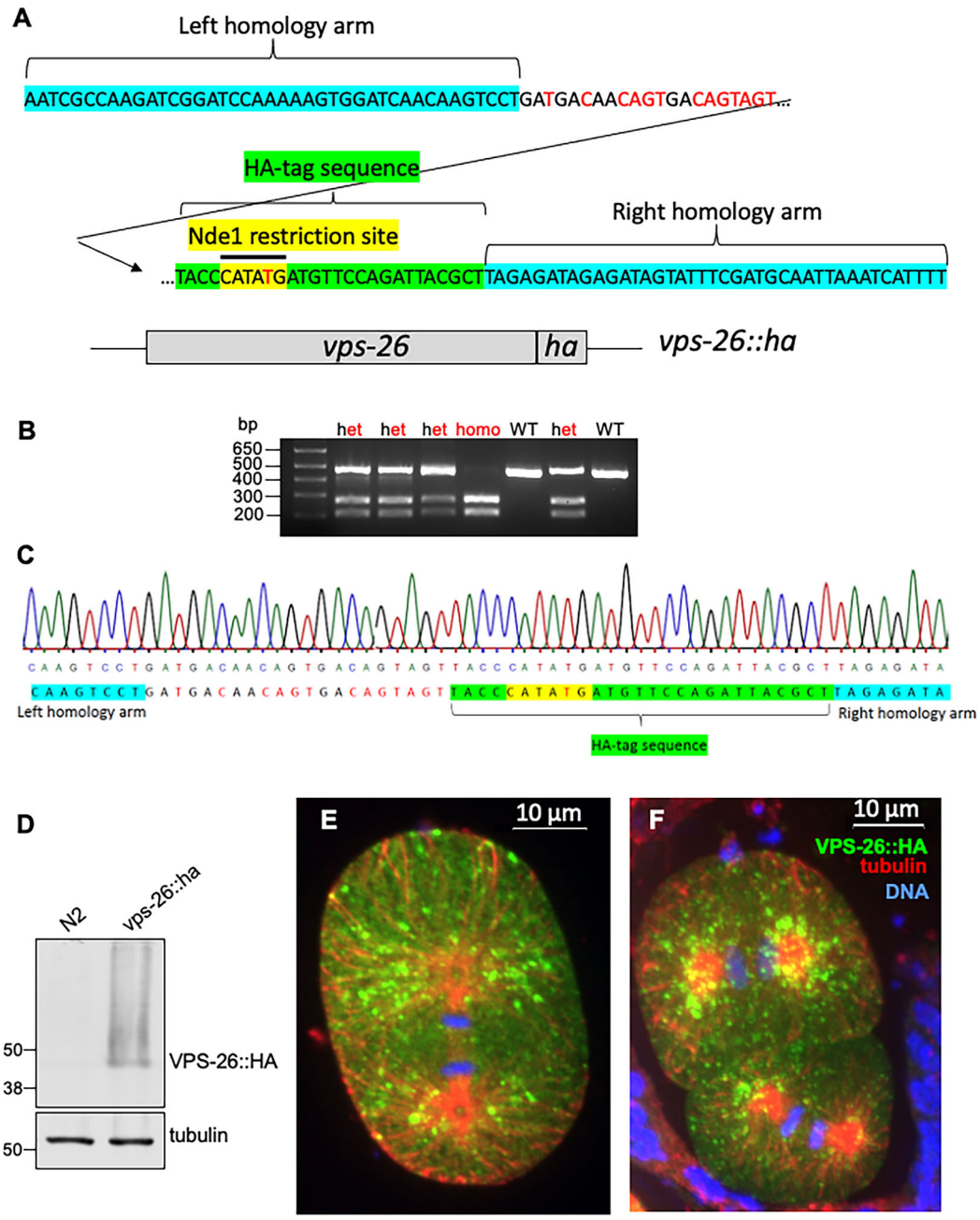

Fig. 1. Expression and validation of VPS-26 expression in *C. elegans*. (A) Schematic of the CRISPR repair template used for inserting a HA tag sequence at the 3′ end of the *C. elegans vps-26* gene. (B) Agarose gel electrophoresis of NdeI-digested PCR products to screen for homozygous-edited *C. elegans* carrying the *vps-26::ha* edit. Het, heterozygote; homo, homozygote; WT, wild-type. (C) Alignment of sequencing data from an identified *vps-26::ha* homozygous worm line with the designed CRISPR repair template demonstrating successful introduction of the HA tag DNA sequence at the 3′ end of the *vps-26* gene. (D) Immunoblot analysis showing VPS-26::HA expression in homozygous edited worms (right lane). The wild-type N2 strain served as a negative control for the experiment (left lane). α-tubulin was used as the loading control. (E,F) Immunofluorescence staining showing VPS-26::HA expression in early *C. elegans* embryos. Green, VPS-26::HA; red, microtubules stained with α-tubulin; blue: DNA. (E) VPS-26::HA expression in a one-cell anaphase *C. elegans* embryo (F) VPS-26::HA expression in a two-cell *C. elegans* embryo. The anterior cell is in telophase whereas the posterior cell is in anaphase. Images are representative of three experiments. Scale bars: 10 µm.

vps-26-knockout worms have a decreased number of progeny, but normal viability

To determine the effect of depleting the retromer complex subunit VPS-26 on *C. elegans* development, brood counts and embryonic viability assays were performed. Brood count assays performed at 20°C showed that *vps-26*-knockout worms had a markedly reduced mean brood size of 18 (n=50) as compared with a mean brood size of 207 in control *vps-26::ha* worms (n=20) (two-tailed unpaired t-test, P<0.0001) (Fig. 3A).

Although the brood size of *vps-26*-knockout worms was reduced by more than 10-fold compared to the control strain, nevertheless almost all the eggs that were laid by the *vps-26*-knockout worms were viable (Fig. 3B). Specifically, the mean embryonic viability of *vps-26*-knockout worms was 99.76% (number of progeny analyzed=918), which was almost indistinguishable from the mean embryonic viability of the control *vps-26:ha* worms, which was 99.05% (number of progeny analyzed=4148) (two-tailed unpaired t-test, P=0.0154) (Fig. 3B). These data indicate that

Journal of Cell Science (2022) 135, jcs259396. doi:10.1242/jcs.259396

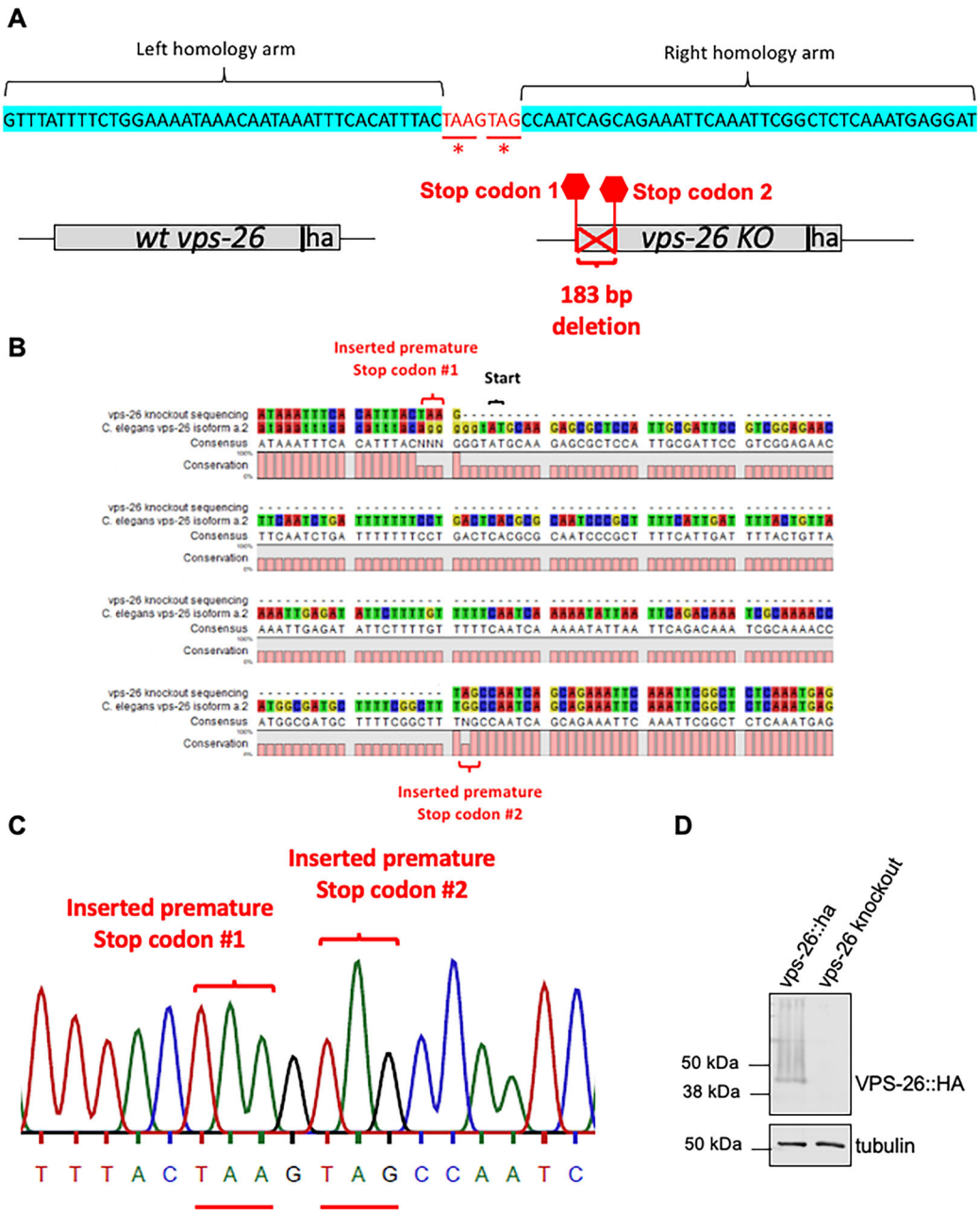

Fig. 2. Deletion of *vps-26* in *C. elegans*. (A) Schematic of the CRISPR repair template used to knockout *C. elegans* VPS-26. (B) Alignment of sequencing data obtained from an identified *vps-26* deletion homozygote with the wild-type *vps-26* gene sequence confirming the insertion of the designed repair template into the *vps-26* gene. (C) Sequencing data obtained from *vps-26*-knockout worms demonstrating successful insertion of the two premature stop codons into the *vps-26* gene via the CRISPR repair template. (D) Western blot showing that VPS-26::HA protein expression was undetectable in the *vps-26*-knockout worms, indicating that the knockout was successfully generated. The *vps-26::ha* strain served as a positive control for the experiment and α-tubulin was used as the loading control.

VPS-26 function is critical for the maintenance of normal brood size but dispensable for embryonic viability.

vps-26-knockout worms display decreased body length compared to normal counterparts

We next examined whether defective vulva development might be responsible for the significantly reduced brood size observed in the *vps-26*-knockout worms. Upon differential interference contrast imaging of control and *vps-26*-knockout worms, we observed that the knockout worms frequently displayed defects in vulva development (Fig. S1). Specifically, a high proportion of the *vps-26*-knockout worms displayed a protruding vulva, which precluded them from laying eggs (Fig. S1B). In worms with a protruding vulva, this likely leads to the build-up and subsequent hatching of eggs inside their uterus, which subsequently causes the parent worm to die, thereby reducing the overall brood size.

Initial cursory examination of *vps-26*-knockout worms through a dissecting microscope suggested that they may be smaller in size than their wild-type counterparts. Therefore, a thorough characterization of wild-type and *vps-26*-knockout worm lengths was performed (Fig. 3C–E). The mean body length of the *vps-26*-knockout worms was 475 µm (n=37) compared to 524 µm (n=30) for the control *vps-26::ha* worms (n=30) (two-tailed unpaired t-test, P<0.0001) (Fig. 3E). These data indicate that VPS-26 function is

Journal of Cell Science

Journal of Cell Science (2022) 135, jcs259396. doi:10.1242/jcs.259396

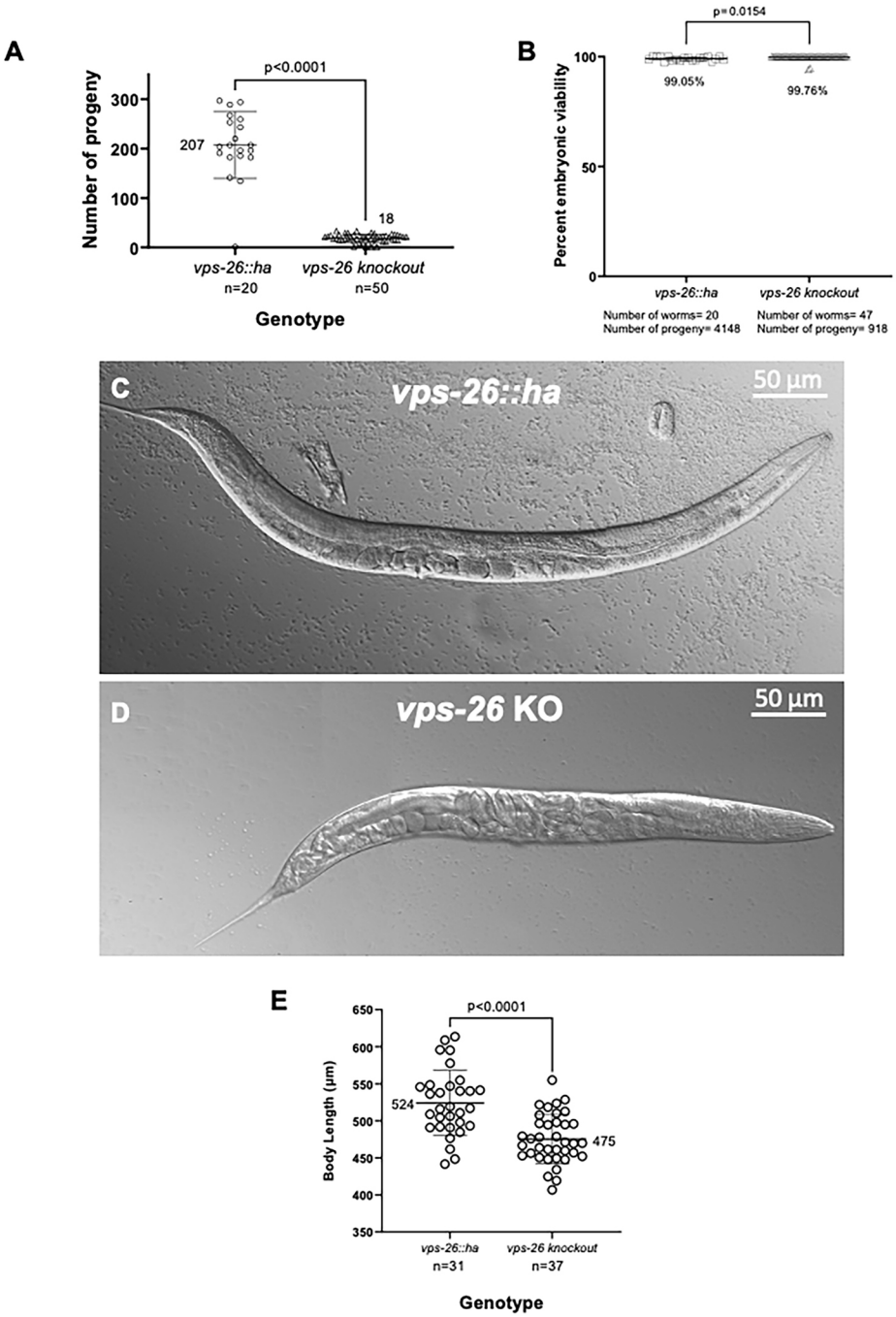

Fig. 3. Effect of *vps-26*-knockout on *C. elegans* brood size, embryonic viability and body length. (A) Quantification of brood sizes of *vps-26::ha* and *vps-26*-knockout worms. The *vps-26*-knockout worms exhibited a significantly reduced average brood size of 18 compared to an average brood size of 207 by control *vps-26::ha* worms at 20°C. *P*<0.0001 (unpaired two-tailed *t*-test). *n*=number of worms whose brood was analyzed for each genotype. (B) Quantification of embryonic viability of *vps-26::ha* and *vps-26*-knockout worms. No significant change in embryonic viability was observed at 20°C upon the depletion of VPS-26. *P*=0.0154 (unpaired two-tailed *t*-test). Error bars represent the mean±s.d. (C) A representative differential interference contrast (DIC) image showing the body length of a control VPS-26::HA worm. (D) A representative DIC image showing the body length of a *vps-26*-knockout worm. Scale bars: 50 µm. (E) Quantification of body lengths of *vps-26::ha* and *vps-26*-knockout worms. *vps-26*-knockout worms have a shorter body length than *vps-26::ha* worms. The mean body length of *vps-26*-knockout worms is 475 µm compared to 524 µm for control *vps-26::ha* worms. *P*<0.0001 (unpaired two-tailed *t*-test). *n*=number of independent worms whose body lengths were measured for each genotype. Error bars represent the mean±s.d.

essential for development and/or maintenance of normal body length in *C. elegans.*

Initial analysis of phasmid neurons in *vps-26*-knockout worms did not reveal primary ciliogenesis defects

A previous study indicated that decreased body size in *C. elegans* is often associated with ciliogenesis defects (Fujiwara et al., 2002). Moreover, since the retromer binding partners EHD1 (Gokool et al., 2007) and MICAL-L1 (Zhang et al., 2012b,c) have already been implicated in regulating ciliogenesis in mammalian cells (Lu et al., 2015; Xie et al., 2019), we then used our *vps-26*-knockout worms to make an initial assessment of whether the retromer complex is required for primary ciliogenesis in worms. To this aim, we crossed *vps-26*-knockout worms with *osm-6p::gfp* worms (Fig. 4A,B), which express soluble GFP from an *osm-6* promoter that labels *C. elegans* sensory neuronal cilia (Bayer et al., 2020). Owing to the extremely low brood numbers for the *osm-6p::gfp; vps-26*-knockout worms, we were able to examine ciliary length only for phasmid neurons. As shown in Fig. 4C–F, we did not detect significant differences in phasmid neuron ciliary length in the *vps-26*-knockout worms, analyzing both the length of the longer phasmid cilia (Fig. 4C; examples shown in E and F), or the length of the shorter phasmid cilia (Fig. 4D). However, given that it has previously been shown that ciliary transition zone defects do not significantly perturb ciliary length or intraflagellar transport (IFT) in the *C. elegans* phasmid cilia (Schouteden et al., 2015), these initial experiments do not preclude potential defects in the ciliary transition zone in *vps-26*-knockout worms. Furthermore,

Journal of Cell Science (2022) 135, jcs259396. doi:10.1242/jcs.259396

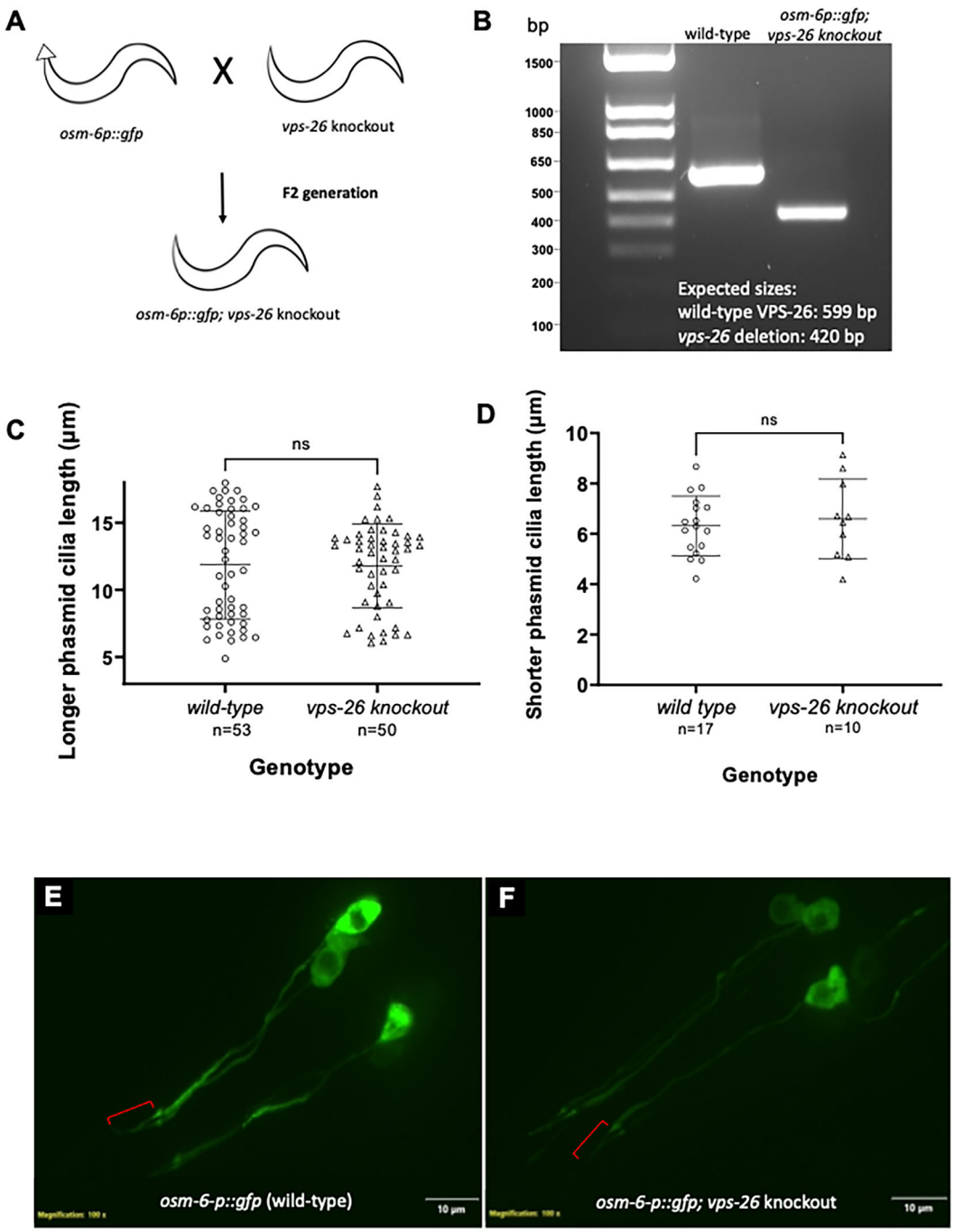

Fig. 4. Phasmid cilia length is unchanged in *vps-26*-knockout worms. (A) Schematic for generating the IYR025 strain expressing soluble GFP from an *osm-6* promoter in the *vps-26*-knockout background. (B) PCR confirmation of introduction of the *vps-26* deletion allele into the PY6100 strain expressing GFP from an *osm-6* promoter. (C) Lengths of the longer of the two phasmid cilia are unaffected in *vps-26*-knockout worms. A scatter plot comparing the lengths of the longer of the two phasmid cilia in wild-type (*osm-6p::gfp*) and IYR025 (*osm-6p::gfp; vps-26*-knockout*)* strains. An unpaired two-tailed *t*-test was used to determine the statistical significance of the data. Error bars represent the mean±s.d. (D). Lengths of the shorter of the two phasmid cilia are unaffected in *vps-26*-knockout worms. A scatter plot comparing the lengths of the shorter of the two phasmid cilia in wild-type (*osm-6p::gfp*) and IYR025 (*osm-6pgfp; vps-26*-knockout) strains. An unpaired two-tailed *t*-test was used to determine the statistical significance of the data. Error bars represent the mean±s.d. (E) Representative image of phasmid cilia from *osm-6p::gfp* expressing wild-type worms. (F) Representative image of phasmid cilia from *osm-6p::gfp* expressing *vps-26*-knockout worms. The red brackets demarcate the longer cilium length. Images representative of three experiments. Scale bars: 10 µm.

there may be other neuron-specific defects or defects in IFT that are not analyzable by the strain that we have constructed. Unfortunately, given the extremely low brood size and vulval defects exhibited by *vps-26*-knockout worms, additional crosses and/or tests to study neuron-specific effects of this mutation are not feasible.

Although we were unable to clarify whether *vps-26*-knockout worms have ciliogenesis defects due to the challenges posed by the developmental effects of VPS-26 depletion, the smaller body sizes of the *vps-26*-knockout worms indicated the existence of potential ciliogenesis defects upon retromer depletion (Fujiwara et al., 2002). Therefore, to more thoroughly characterize the role of the retromer

Journal of Cell Science (2022) 135, jcs259396. doi:10.1242/jcs.259396

complex subunits in ciliogenesis, we used RPE-1 cells as a model system for our remaining ciliogenesis experiments.

Retromer complex subunits are required for normal primary ciliogenesis

To determine whether the retromer complex is required for the generation of the primary cilium, we first depleted RPE-1 cells of all three different retromer core complex subunits, VPS26, VPS35 or VPS29, using siRNA oligonucleotides (Fig. 5D,H). We then induced primary ciliogenesis by serum starvation and assessed the generation of the cilia after marking them with an antibody against acetylated tubulin (Fig. 5A–C,F,G; arrows denote primary cilia). Although ∼50% of mock-treated RPE-1 cells formed primary cilia (Fig. 5A,F, see arrows marking cilia, and quantified in Fig. 5E,I), reduced expression of either VPS26, VPS35 or VPS29 resulted in a greater than two-fold decrease in the number of ciliated RPE-1 cells (compare Fig. 5A to B and C, quantified in E; compare Fig. 5F to G, quantified in I).

Given that in mammalian cells, the VPS26–VPS29–VPS35 heterotrimer loosely binds to different sorting nexin dimers, which can function independently of the core complex (Kvainickas et al., 2017; Simonetti et al., 2017), we also examined the role of the affiliated SNX1, SNX2 and SNX5 proteins in ciliogenesis using siRNA (Fig. 6). Indeed, whereas ∼50% of mock-treated cells were ciliated (Fig. 6A,E, see arrows marking cilia; quantified in Fig. 6D, I), upon depletion of SNX1, SNX2 or SNX5, only ∼10% of cells were detected with cilia (compare Fig. 6A to B and Fig. 6E to F,G; quantified in Fig. 6D,I). An additional sorting nexin protein implicated in recycling from the endosome, SNX27 (Gallon et al., 2014; Lauffer et al., 2010), similarly impaired primary ciliogenesis when depleted from RPE-1 cells (Fig. S2). These data provide evidence that the retromer complex, including the VPS26–VPS29–VPS35 heterotrimer and affiliated sorting nexin proteins, is required for ciliogenesis in mammalian cells.

The retromer complex localizes to the primary cilium

Given the involvement of retromer in ciliogenesis, we next assessed whether retromer localizes to the membrane of the primary cilium and/or ciliary pocket. To address this, serum-starved RPE-1 cells were immunostained with antibodies to acetylated-tubulin to mark cilia, and with antibodies to VPS35 to evaluate the localization of the retromer complex (Fig. 7A). In ciliated cells, endogenous VPS35 was indeed detected at the base of the cilium (arrowhead), potentially at the ciliary pocket membrane, as well as on the daughter centriole (arrow), but not along the length of the cilium (Fig. 7A, dashed oval marks the centrioles).

Recruitment of VPS35 to the centrosome is independent of MICAL-L1 and EHD1

Both EHD1 and MICAL-L1 interact with the retromer complex (Gokool et al., 2007; Zhang et al., 2012b,c). MICAL-L1 is recruited to the centrosome through an interaction with tubulin, and EHD1 is recruited by MICAL-L1 (Xie et al., 2019). Both MICAL-L1 and EHD1 are required for the generation of primary cilia (Lu et al., 2015; Xie et al., 2019). Given that we observed localization of VPS35 to the primary cilium, we asked whether retromer is recruited onto the ciliary base and/or the centrioles through its association with MICAL-L1 and/or EHD1. Accordingly, we used siRNA to deplete RPE-1 cells of MICAL-L1 or EHD1 (Fig. 7D), and immunostained for acetylated tubulin and endogenous VPS35 (Fig. 7B,C). As expected upon serum starvation, and as previously published (Lu et al., 2015; Xie et al., 2019), ciliogenesis was impaired in the absence of EHD1 or MICAL-L1 (compare Fig. 7A to B,C). However, despite the lack of a primary cilium in most cells lacking EHD1 or MICAL-L1, VPS35 was nonetheless observed at the centrioles of these non-ciliated cells (Fig. 7B,C,E; dashed ovals mark the VPS35 localized to centrioles).

Given the consistent localization of VPS35 to the mother and daughter centrioles, we questioned whether retromer might be required for recruitment of MICAL-L1 and EHD1 to the centrioles and primary cilium. Accordingly, we used siRNA oligonucleotides to deplete expression of either VPS35 or VPS26 in both RPE-1 cells and CRISPR/Cas9 gene-edited NIH3T3 cells expressing endogenous levels of EHD1–GFP (Fig. 7I,N). As previously reported, depletion of one retromer core complex subunit also decreased expression of the other subunit (Arighi et al., 2004), consistent with the notion that the complex becomes destabilized when any subunit is missing. Significantly, reduced expression of either VPS26 or VPS35 did not alter recruitment of MICAL-L1 to centrioles in RPE-1 cells (Fig. 7F–H; quantified in Fig. 7J) or EHD1–GFP to centrioles in NIH3T3 cells (Fig. 7K–M; quantified in Fig. 7O).

VPS26 and VPS35 are required for CP110 removal from the mother centriole to facilitate ciliogenesis

A key step in the process of primary ciliogenesis is the removal of the centriolar capping protein CP110 from the mother centriole, thus facilitating the assembly of ciliary vesicles (Lu et al., 2015). To further our understanding of the mechanism by which retromer regulates ciliogenesis, we asked whether retromer plays a role in removal of CP110 from the mother centriole during the early stages of ciliogenesis and depleted VPS35 and VPS26 from RPE-1 cells with siRNA oligonucleotides (Fig. 8E). Indeed, whereas ∼80% of mock-treated cells displayed CP110 loss from the mother centriole (Fig. 8A, see dashed oval; quantified in Fig. 8D), CP110 removal was detected in less than 60% of cells depleted of VPS26 (Fig. 8B; quantified in Fig. 8D) or VPS35 (Fig. 8C; quantified in Fig. 8D). Although the decrease in CP110 removal was typically ∼25%, it nonetheless suggests a role for retromer in a relatively early stage of ciliogenesis. Indeed, it was of interest that whereas loss of CP110 from the mother centriole in mock-treated cells almost always led to subsequent cilia generation, in the VPS35- and VPS26-depleted cells loss of CP110 did not strictly correlate with ciliogenesis. This suggests that retromer may have additional functions in later steps of ciliogenesis, potentially in coordination with Rab8 function. Moreover, consistent with our previous findings that neither EHD1 nor MICAL-L1 is required for the recruitment of myosin Va-positive preciliary vesicles to the distal appendages (Xie et al., 2019), depletion of neither VPS26 nor VPS35 had an effect on preciliary vesicle movement to the centriolar distal appendages (Fig. S3A–C; quantified in Fig. S3D).

Although the mechanisms by which CP110 is removed from the mother centriole upon ciliogenesis are complex and poorly delineated, we aimed to increase our knowledge of the mode by which retromer might potentially regulate this step. Accordingly, we hypothesized that retromer might associate with CP110. To this end, we performed immunoprecipitations of cell lysates using antibodies directed to CP110, and we immunoblotted with antibodies against VPS35 and VPS26. As shown, we detected bands representing both VPS35 and VPS26, but these bands were absent when a control antibody (anti-GFP) was used for immunoprecipitation (Fig. 8F), suggesting that CP110 can reside in a complex with retromer. In addition, we also showed that a pool of endogenous VPS35 localized to CP110-labeled centrioles (Fig. 8G). Indeed, both confocal imaging and structured

Journal of Cell Science (2022) 135, jcs259396. doi:10.1242/jcs.259396

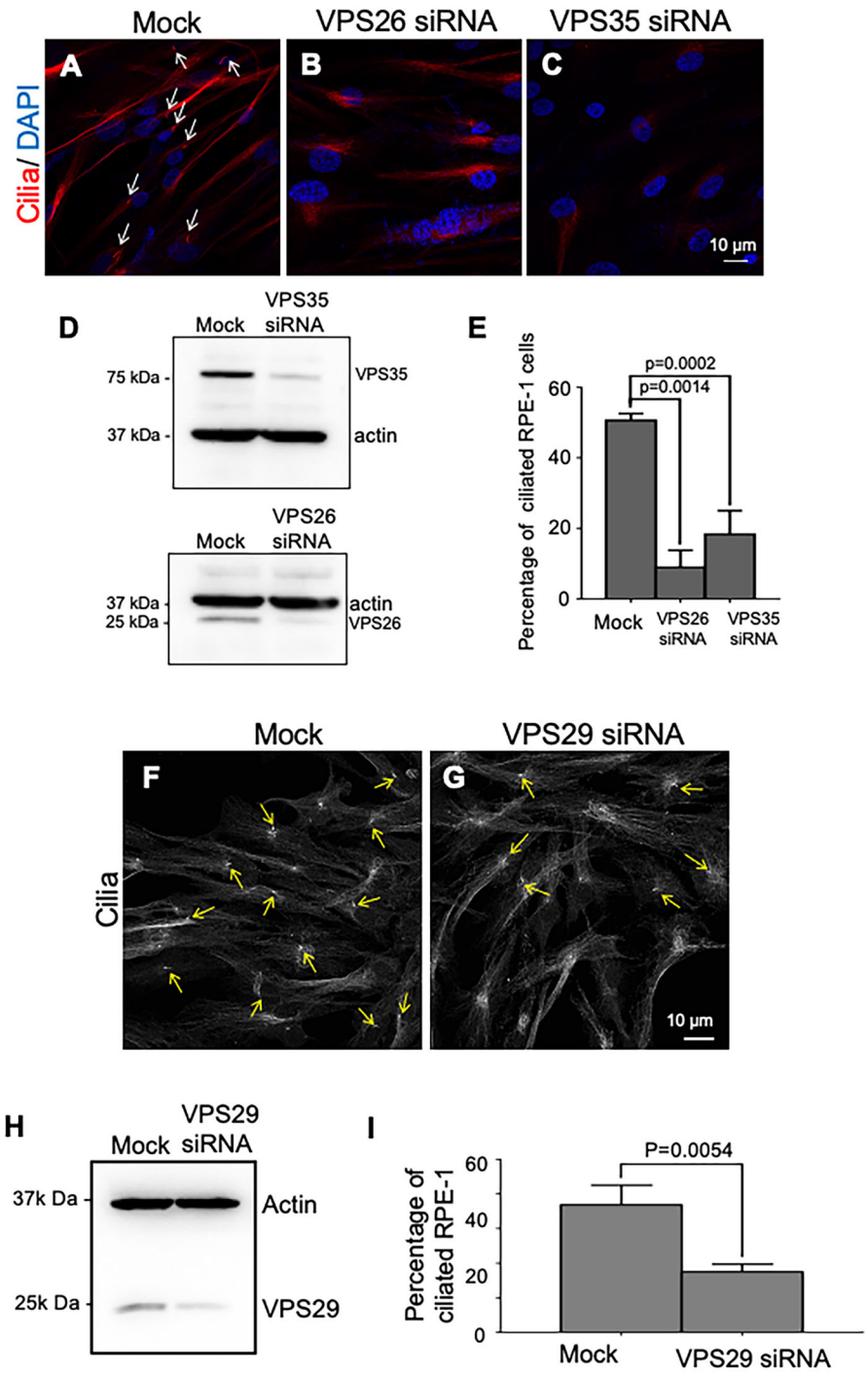

Fig. 5. VPS26, VPS35 and VPS29 are required for normal ciliogenesis. (A–E) RPE-1 cells were mock-treated (with Lipofectamine RNAi-MAX in the absence of siRNA oligonucleotides), or treated with VPS26 or VPS35 siRNA for 48 h. Cells were then serum starved for 24 h to induce ciliogenesis. Immunofluorescence staining of acetylated tubulin reveals cilia (marked by white arrows). Compared to mock-treated cells (A), fewer cilia were generated upon depletion of VPS26 (B) or VPS35 (C). VPS26 and VPS35 siRNA-depletion efficacies were determined by immunoblotting (D). The percentages of ciliated RPE-1 cells from either mock- or siRNA-treated cover-slips were quantified and are presented as a bar graph (E). (F–I) RPE-1 cells were either mock-treated or treated with VPS29 siRNA for 48 h, followed by serum starvation for 24 h to induce ciliogenesis. Cells were then fixed and immunostained for acetylated tubulin to reveal cilia (denoted by yellow arrows). Compared to mock (F), fewer cilia were detected in cells depleted of VPS29 (G). VPS29 knockdown efficacy was demonstrated by immunoblotting (H), and the percentage of ciliated cells mock-treated or treated with was quantified and presented as a bar graph (I). *P*-values were calculated for comparison between mock- and siRNA-treated cells (unpaired two-tailed *t*-test); $n=3$ experiments (>100 cells quantified for each experiment). Error bars denote s.d. Images in A–D, F–H representative of three experiments.

illumination imaging showed VPS35 localized to both mother and daughter centrioles (Fig. 8H), although more precise information on its localization within the centriolar region will require either single-molecule super-resolution imaging or electron microscopy. On the other hand, neither SNX1 nor SNX2 were detected in immune complexes with CP110, nor were they observed localized to centrioles or in the proximity of CP110 (Fig. S4). These data further support the notion that the core retromer subunits VPS26, VPS35 and likely VPS29 form a complex with CP110 to facilitate its removal from the mother centriole, whereas the more loosely associated ESCPE-1 complex sorting nexins play a more indirect role in regulating ciliogenesis.

DISCUSSION

Although initially characterized for its role in retrieval of the yeast Vps10p (Seaman et al., 1997) and the mammalian cation-independent mannose-6-phosphate receptor to the Golgi complex (Arighi et al., 2004), recent studies suggest that retromer core complex subunits play crucial roles in regulating neuronal mitochondria function, and mutations in the VPS35 subunit have been linked to Parkinson's disease (Braschi et al., 2010; Follett et al., 2014; Vilariño-Güell et al., 2011; Zimprich et al., 2011). Advances in understanding the retromer complex have come from cryo-electron tomography studies and provide evidence for a scaffolding structure in which the VPS26, VPS35 and VPS29 core subunits form

Journal of Cell Science (2022) 135, jcs259396. doi:10.1242/jcs.259396

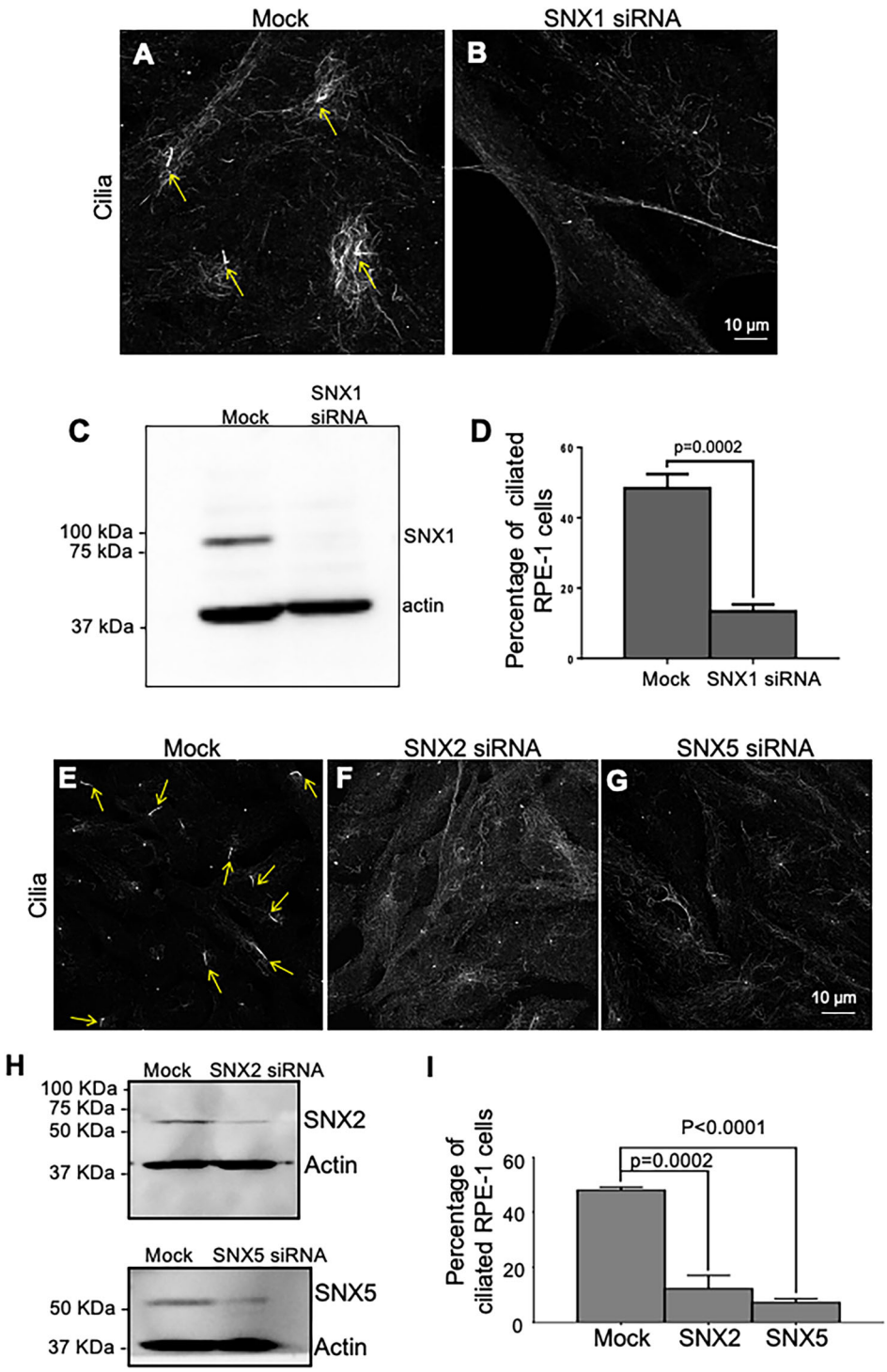

Fig. 6. SNX1, SNX2 and SNX5 are required for normal ciliogenesis. (A–D) RPE-1 cells were mock-treated (with Lipofectamine RNAi-MAX in the absence of siRNA oligonucleotides), or treated with SNX1 siRNA for 48 h. Cells were then serum starved for 24 h to induce ciliogenesis. Immunofluorescence staining of acetylated tubulin reveals cilia (marked by yellow arrows). Compared to mock-treated cells (A), fewer cilia were generated upon depletion of SNX1 (B). SNX1 siRNA depletion efficacy was determined by immunoblotting (C). The percentages of ciliated RPE-1 cells from either mock- or siRNA-treated coverslips were quantified and are presented as a bar graph (D). (E–I) RPE-1 cells were either mock-treated or treated with SNX2 or SNX5 siRNA for 48 h, followed by serum starvation for 24 h to induce ciliogenesis. Cells were then fixed and immunostained for acetylated tubulin to reveal cilia (denoted by yellow arrows). Compared to mock (E), fewer cilia were detected in cells depleted of either SNX2 (F) or SNX5 (G). SNX2 and SNX5 knockdown efficacies were demonstrated by immunoblotting (H), and the percentage of ciliated mock-treated, SNX2 siRNA and SNX5 siRNA depleted cells was quantified and presented as a bar graph (I). *P*-values were calculated for comparison between mock- and siRNA-treated cells (unpaired two-tailed *t*-test); $n=3$ experiments (>100 cells quantified for each experiment). Error bars denote s.d. Images in A–C, E–H representative of three experiments.

an arch that extends from the membrane, and the VPS5 subunit (the yeast homolog of mammalian SNX1) assembles on the lipid bilayer of the endosome (Kovtun et al., 2018). However, unlike in yeast, the mammalian retromer may have evolved to function more loosely in coordination with the SNX dimers so that the cation-independent mannose-6-phosphate receptor requires involvement of the heterodimeric ESCPE-1 complex (SNX1 or SNX2 and either SNX5 or SNX6) (Evans et al., 2020; Simonetti et al., 2019), although this remains somewhat controversial (Seaman, 2021).

Although a recent study has elucidated the structure of the metazoan and fungal retromer complexes (Leneva et al., 2021), and various new studies have addressed retromer in *Drosophila* (Walsh et al., 2021; Ye et al., 2020), fewer studies have addressed retromer function in invertebrate organisms such as *C. elegans*. We chose to address the role of the worm VPS-26 protein based on its high level of amino acid identity with its mammalian VPS26 counterpart (58% identity to the *Homo sapiens* protein). Moreover, since knockdown of a single retromer core complex subunit leads to the degradation of the other subunits (Arighi et al., 2004) and given the homology between retromer core complex structures of different organisms (Leneva et al., 2021), it is fair to assume that knockout of *C. elegans vps-26* gene leads to a dysfunctional worm retromer complex.

Journal of Cell Science (2022) 135, jcs259396. doi:10.1242/jcs.259396

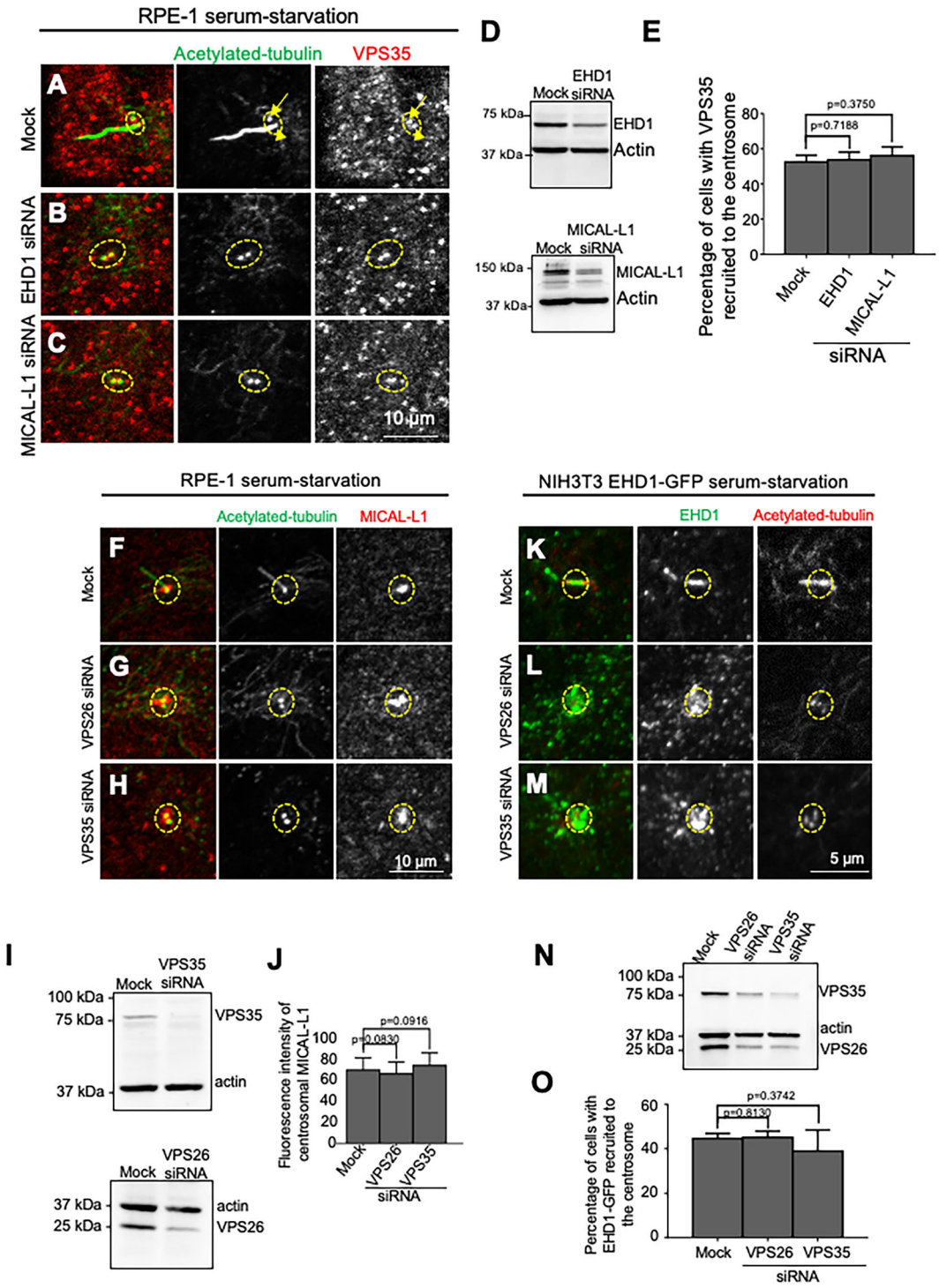

Fig. 7. See next page for legend.

We found that VPS-26 and retromer likely regulate worm development, as the number of progeny produced per worm was dramatically reduced by more than 10-fold, potentially as a result of impaired vulva formation often marked by a protruding vulva (Fig. S1). It is noteworthy that the *C. elegans* hermaphrodite vulva is considered a unique model for the study of signaling molecule trafficking within the cell (Schmid and Hajnal, 2015), leading us to speculate that retromer-controlled protein transport might explain the vulval defects seen in *vps-26*-knockout worms. In the future, additional studies should be conducted to determine the mechanism by which inhibition of the retromer complex subunits causes vulval defects.

Our studies with a *vps-26* deletion allele generated using CRISPR/Cas9 editing demonstrate that the complete knockout of *vps-26* does not decrease embryonic viability as compared with the control strain (Fig. 3B). However, a previous study which investigated the role of the retromer complex in regulating Wnt gradient formation in *C. elegans* reported in the supplementary data

Journal of Cell Science (2022) 135, jcs259396. doi:10.1242/jcs.259396

Fig. 7. VPS35 is recruited to the basal body/centrioles independently of MICAL-L1 and EHD1, and retromer is non-essential for the recruitment of MICAL-L1 and EHD1 to the centrosome. (A–E) RPE-1 cells were mock treated (A), or treated with EHD1 siRNA (B) or MICAL-L1 siRNA (C), and then serum starved for 1 h to induce ciliogenesis. Cells were fixed and immunostained with antibodies to acetylated tubulin to mark cilia and/or centrioles (green) and VPS35 (red). VPS35 localized to both mother (yellow arrowheads) and daughter centrioles (yellow arrows) in mock-treated and siRNA-treated cells (A–C, dashed ovals). The efficacy of EHD1 and MICAL-L1 knockdown was determined by immunoblotting (D). Bar graph representing the percentage of cells with VPS35 detectable at the centrosome in mock-treated cells, or cells depleted of EHD1 or MICAL-L1 (E). Retromer is non-essential for the recruitment MICAL-L1 and EHD1 to the centrosome. (F–J) Mock-treated (F), VPS26-siRNA-treated (G) or VPS35-siRNA-treated (H) RPE-1 cells were serum starved for 1 h to induce ciliogenesis. The cells were then fixed and immunostained for acetylated tubulin (green) to reveal cilia and/or centrioles, and for MICAL-L1 (red) to reveal its localization (F–H). MICAL-L1 was detected on acetylated-tubulin-labeled cilia/centrioles in both mock-treated (F) and VPS26-depleted (G) and VPS35-depleted (H) cells. VPS35 and VPS26 depletion by siRNA was demonstrated by immunoblotting (I). A circular region of interest (ROI) of 1.57 µm in diameter was projected around the basal body or mother centriole. The fluorescence intensity of the MICAL-L1 immunostaining within this ROI was measured and is presented as a bar graph (J). (K–O) CRISPR/Cas9 gene-edited NIH3T3 cells expressing EHD1–GFP were mock-treated (K) or treated with either VPS26 siRNA (L), or VPS35 siRNA (M), serum starved for 1 h, and immunostained for acetylated tubulin (red) or with anti-GFP antibodies to reveal EHD1 localization (green). EHD1 localized to acetylated-tubulin-labeled cilia/centrioles in mock-treated (K) and VPS26-depleted (L) and VPS35-depleted (M) cells. VPS35 and VPS26 depletion in NIH3T3 gene-edited cells by siRNA was demonstrated by immunoblotting (N). Recruitment of EHD1 to the centrosome was determined by projecting a ROI of 1.57 µm in diameter around the basal body or mother centriole and measuring the fluorescence intensity of EHD1 immunostaining within this ROI (O). *P*-values were calculated for comparison between mock- and siRNA-treated cells (unpaired two-tailed *t*-test); n=3 experiments (>100 cells quantified for each experiment). Yellow dashed ovals denote the ROIs and region of the centrioles. Error bars denote s.d. Images in A–D, F–I, K-N representative of three experiments.

section that the *vps-26(tm1523)* mutant strain exhibits 32% embryonic lethality (Coudreuse et al., 2006). The *vps-26(tm1523)* mutation causes a premature stop codon in the VPS-26 protein, leaving the N-terminal 72 amino acids intact. Thus, this mutation is expected to be a strong loss-of-function mutation, if not a null mutation. The differences in the embryonic lethality data obtained with the two strains could be explained by potential background mutations that could be present in the *vps-26(tm1523)* strain resulting from the mutagenesis used to generate the knockout allele (*C. elegans* Deletion Mutant Consortium, 2012). Thus, our data highlight the advantages of using CRISPR/Cas9 editing to unambiguously establish *C. elegans* mutant phenotypes.

Another significant developmental difference observed in *vps-26*-knockout worms was in body length, with the knockout worms consistently displaying shorter body lengths (Fig. 3C–E). Interestingly, knockdown of the retromer subunit protein VPS-35 in *Xenopus tropicalis* using morpholinos also resulted in decreased body length (Coudreuse et al., 2006), suggesting that retromer may play an evolutionarily conserved role in maintaining proper body length. Intriguingly, a smaller worm body length has been previously associated with ciliogenesis defects (Fujiwara et al., 2002). Knockout of other related endocytic regulatory proteins, such as SNX3, similarly lead to decreased brood size and worm length (Vieira et al., 2018). Future studies should be directed towards dissecting the mechanism by which the retromer complex functions to maintain a normal body length.

Low brood numbers, such as we observed in our *vps-26*-knockout worms, can also be correlated with defects in ciliogenesis, albeit in a 3D culture environment (Lee et al., 2016). Moreover, a recent study indicates that ciliogenesis in *C. elegans* BAG sensory neurons is coordinated by retromer-mediated vesicular trafficking (Martinez-Velazquez and Ringstad, 2018). Dye-filling assays have been previously performed in three retromer mutants, displaying defects of 4% for the *vps-35*(*hu68*) allele, 2% for the *vps-29*(tm1320) allele and 0% for the *vps-26*(*tm1523*) allele (Coudreuse et al., 2006). Although these data suggest that there may not be severe ciliogenesis defects with single retromer knockouts, it is possible that in worms there is a redundancy in function of the retromer complex proteins in regulating ciliogenesis. In future studies it will be interesting to determine if simultaneously depleting two or more members of the retromer complex produces more robust ciliogenesis defects in worms. Moreover, the data obtained in the Coudreuse et al. (2006) study for the *vps-26(tm1523)* allele is in line with our recent findings showing that the knockout of *vps-26* does not affect phasmid ciliary length, which indicates that this mutant does not exhibit severe defects in ciliogenesis. However, as ciliary length is relatively unaffected in *C. elegans* transition zone mutants, we cannot exclude potential defects in the transition zone assembly or in intraflagellar trafficking in our *vps-26*-knockout worms. Further, dye-filling assays only examine ciliogenesis in a subset of the *C. elegans* sensory neurons. Accordingly, it will be interesting to determine whether neuron-specific ciliogenesis defects exist in different retromer mutants. Unfortunately, owing to the severe vulval defects and low brood sizes of the *vps-26*-knockout worms, we were unable to perform these investigations with the *vps-26*-knockout worms.

Several recent studies in mammalian systems hint at the potential involvement of the retromer complex in ciliogenesis. A study in mammalian cells demonstrated that the retromer complex proteins interact with polycystin 2, a ciliary protein whose defects are associated with autosomal dominant polycystic kidney disease (Tilley et al., 2018). An endosomal protein and retromer interaction partner known as SDCCAG3 (also known as ENTR1) (McGough et al., 2014) localizes to the basal body of primary cilia and its depletion impairs ciliogenesis (Hagemann et al., 2013; Yu et al., 2016). Whether SDCCAG3 and the retromer complex cross-talk to regulate ciliogenesis remains an open question. Another study demonstrated that SNX17, a sorting nexin that binds to the retriever complex (which contains VPS29 and homologs of both VPS35 and VPS26; McNally et al., 2017) and is involved in sorting, fission and recycling at the endosome (Dhawan et al., 2020; Donoso et al., 2009; Steinberg et al., 2012; Stockinger et al., 2002), also regulates ciliogenesis (Wang et al., 2019). Collectively, these findings suggest that retromer may regulate ciliogenesis. Although our initial studies in worms did not identify significant differences in phasmid neuron ciliary length, it remains possible that defects in ciliogenesis might be evident in other neuronal cilia. However, we rationalized that evaluating the role of retromer in ciliogenesis would be more practical in mammalian cells.

Our data demonstrate a greater than 2-fold reduction in ciliated mammalian RPE-1 cells upon serum starvation when either VPS26, VPS35 or VPS29 are targeted by siRNA oligonucleotides. Coupled with additional data showing that depletion of SNX1, SNX2 and SNX5 also dramatically reduce primary ciliogenesis, it is evident that both the retromer core complex proteins and the affiliated sorting nexin ESCPE-1 complex contribute to the process. While the VPS26 depletion appears to cause an even more significant reduction in ciliated cells than VPS35 depletion, we anticipate that these differences do not necessarily represent any hierarchy in significance of the retromer proteins, but more likely reflect differential efficiency of retromer core complex subunit depletion by siRNA. Moreover,

Journal of Cell Science (2022) 135, jcs259396. doi:10.1242/jcs.259396

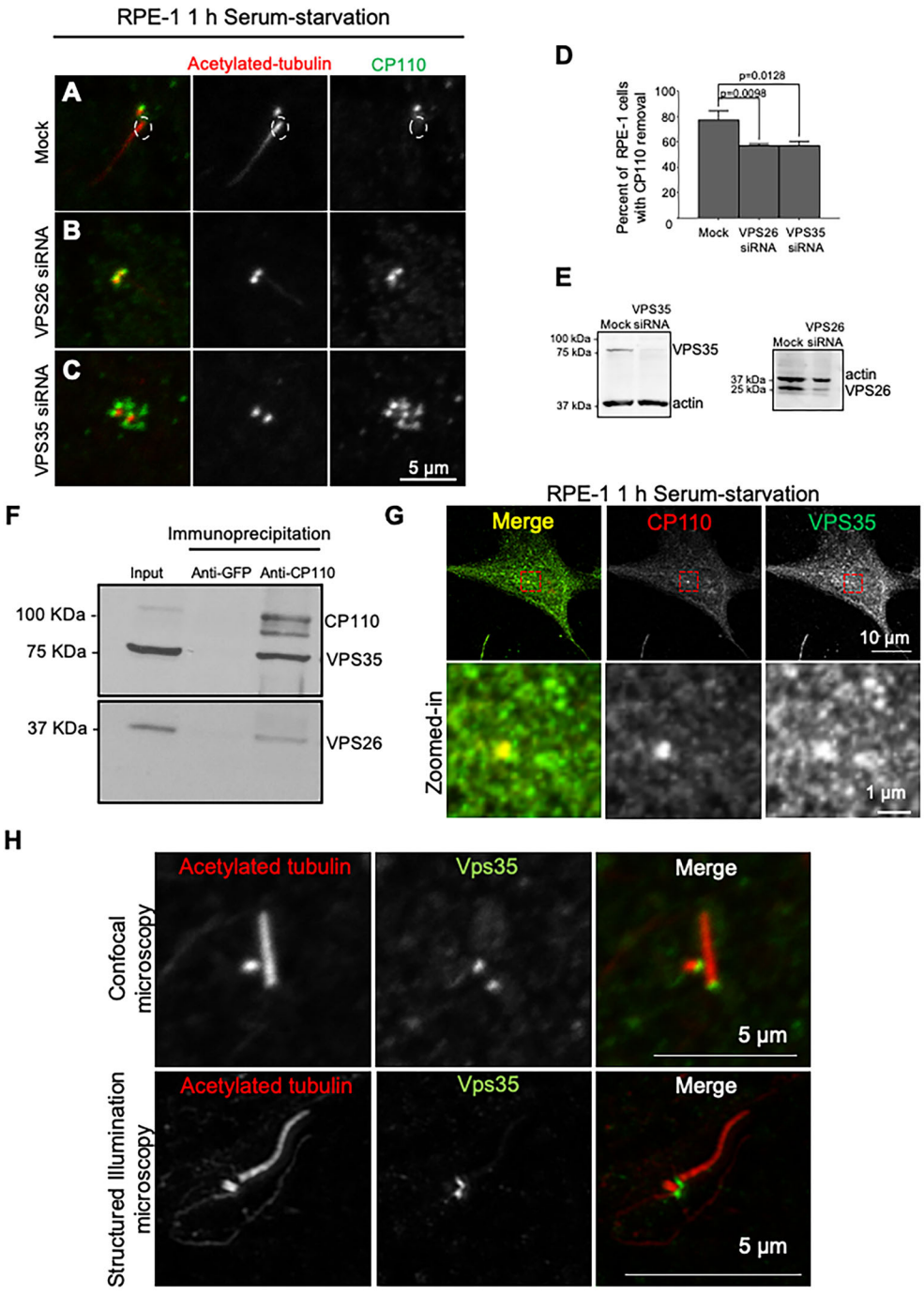

Fig. 8. VPS26 and VPS35 regulate CP110 removal from the mother centriole prior to ciliogenesis. (A–E) Mock-treated (A), VPS26-siRNA-treated (B) and VPS35-siRNA-treated (C) RPE-1 cells were serum starved for 1 h, fixed and immunostained with antibodies targeting acetylated tubulin (red) and CP110 (green). CP110 removal from the mother centriole was impaired upon depletion of VPS26 and VPS35. Bar graph (D) shows the percentage of RPE-1 cells displaying CP110 removal from the m-centriole. *P*-values were calculated for comparison between mock- and siRNA-treated cells (unpaired two-tailed *t*-test); $n=3$ experiments (>100 cells quantified for each experiment). Error bars denote s.d. VPS35- and VPS26-depletion by siRNA was demonstrated by immunoblotting (E). (F) CP110 interacts with VPS26 and VPS35. RPE-1 cell lysates were subjected to immunoblotting (Input, 4%) or immunoprecipitation using anti-CP110 antibodies or rabbit anti-GFP antibodies (negative control). Immunoprecipitated proteins were immunoblotted with anti-CP110, anti-VPS35, and anti-VPS26 antibodies. (G) CP110 displays partial colocalization with VPS35 on the mother centriole. RPE-1 cells were fixed and immunostained using anti-CP110 antibodies (red) and anti-VPS35 antibodies (green). (H) VPS35 partially localizes to acetylated tubulin labeled basal body/cilia. RPE-1 cells were fixed and immunostained using anti-acetylated tubulin antibodies (red) and anti-VPS35 antibodies (green). Immunofluorescence images were taken by confocal microscopy and structured illumination microscopy. Images in A–C, E–H, representative of three experiments.

knocking down one core complex subunit is known to affect expression of the other subunits (Arighi et al., 2004) (Fig. 7N), further complicating any attempts to assign significance to the modest differences observed in ciliogenesis between VPS26 and VPS35 upon their depletion. Overall, however, the data point to a clear requirement for both the retromer core complex and its affiliated SNX dimer or ESCPE-1 complex for normal primary cilia biogenesis, highlighting a common role for both protein assemblages in mammalian cells, at least in the regulation of primary cilia formation.

A number of studies have identified interactions between retromer complex members and other endocytic regulatory proteins, including EHD1 and MICAL-L1 (Gokool et al., 2007; McKenzie et al., 2012; Zhang et al., 2012b,c), and the latter two proteins have been clearly implicated in ciliogenesis and/or localized to the centrosome (Naslavsky and Caplan, 2020; Xie et al., 2019, 2018). However, despite these interactions, retromer, EHD1 and MICAL-L1 appear to be recruited to the basal body/centrioles independently of one another. MICAL-L1 is recruited to the centrosome through its interactions with microtubules, and in turn recruits EHD1 (Xie et al., 2019). How retromer is independently recruited remains to be determined, and potential mechanisms might include through the multitude of proteins that interact with the core complex subunits, in particular VPS35.

Although retromer is recruited to the centrosome/basal body independently of EHD1, retromer acts primarily at an early stage of ciliogenesis similar to EHD1 and MICAL-L1. Removal of the CP110 capping protein from the mother centriole is a critical step in ciliogenesis, and Rab11, EHD1 and MICAL-L1 are required to

Journal of Cell Science (2022) 135, jcs259396. doi:10.1242/jcs.259396

facilitate this event (Feng et al., 2012, 2015; Lu et al., 2015; Xie et al., 2019), whereas Rab8 plays a role later on post-CP110 removal (Knödler et al., 2010). Although the mechanism for CP110 removal is complex and might be regulated by multiple pathways (Goncalves et al., 2021; Hossain et al., 2017; Kobayashi et al., 2011; Lo et al., 2019; Spektor et al., 2007), the interaction we have observed between the retromer core complex proteins VPS26 and VPS35 with CP110 hints at involvement of a potential vesicular transport pathway. Although this remains speculative, one possibility is that endocytic vesicles containing retromer might dock adjacent to the mother centriole, and interactions between retromer and CP110 might facilitate its removal from the centriole. Alternatively, retromer might mediate CP110 removal by a more indirect pathway, such as the transport of E3 ligases to the mother centriole from centriolar satellites to enable CP110 ubiquitination and its subsequent degradation. While the interaction between CP110 and retromer supports the former mechanism, the crucial role of CP110 in ciliogenesis suggests that both mechanisms are not mutually exclusive and that control of CP110 removal from the mother centriole might be regulated in multiple ways. Given the recent involvement of vesicular trafficking in non-endocytic events (Farmer et al., 2017; Naslavsky and Caplan, 2020; Xie et al., 2018), future studies will be aimed at determining the mechanisms by which retromer and EHD1 mediate CP110 removal from the mother centriole.

MATERIALS AND METHODS

C. elegans growth and maintenance

All *C. elegans* strains were grown on MYOB agar plates seeded with OP50 bacteria and maintained at 20°C. The strains used in this study are listed in Table S1.

CRISPR/Cas9 genome editing

CRISPR/Cas9 editing to generate the *vps-26::ha* (IYR010) and *vps-26*-knockout (IYR021) strains was performed using assembled ribonucleoprotein complexes as described previously (Iyer et al., 2019; Smith et al., 2020). The sequences of the primers, guide RNAs and repair templates used for making each strain are listed in Table S2. The *vps-26::ha* strain was generated first in the wild-type N2 background. The *vps-26::ha* strain then served as the background for generating the *vps-26*-knockout strain. All generated strains were confirmed for homozygosity by PCR or by PCR followed by restriction digestion and agarose gel electrophoresis as well as by DNA sequencing.

Preparation of *C. elegans* lysates for immunoblotting

C. elegans lysates for immunoblotting were prepared as follows. Briefly, 100 gravid adults for each genotype were picked into 1 ml of M9 buffer (3 g KH_2PO_4, 6 g Na_2HPO_4, 5 g NaCl, 1 ml 1 M $MgSO_4$ and H_2O to 1 l). The worms were washed twice in 1 ml of M9 buffer by centrifugation at 300 ***g*** for 5 min. The worm pellet was then resuspended in 40 µl of 4× SDS-PAGE sample buffer [0.25 M Tris-HCl pH 6.8, 8% SDS (w/v), 40% glycerol, 20% β-mercaptoethanol and 0.05% (w/v) Bromophenol Blue in distilled water], heated at 95°C for 10 min and stored at −30°C until further use.

Immunoblotting of *C. elegans* lysates

C. elegans lysates were subjected to immunoblotting by using the wet transfer method. Briefly, 10 µl of each worm lysate was loaded onto each well of a 10% Bis-Tris gel. The gels were run at a constant current of 60 to 80 mA for ∼2 h until sufficient band separation was achieved. The proteins were transferred from the gel onto a 0.2 µm nitrocellulose membrane using the wet transfer method (Bio-Rad Laboratories, Hercules, CA). Overnight transfer was performed for 16 h using a constant voltage of 30 V. The membranes were blocked using the Intercept blocking buffer (LI-COR Biosciences, Inc., Lincoln, NE), incubated with rabbit anti-HA (1:1000; Cell Signaling Technology, Danvers, MA; catalog #3724S) and mouse anti-tubulin (1:200; Santa Cruz Biotechnology, Dallas, TX; catalog # sc-32293) antibodies for 2 h and washed three times with 1× Tris-buffered saline, 0.1% Tween 20 (20 mM Tris, 150 mM NaCl, 0.1% Tween 20; TBST). The membranes were then incubated with goat anti-mouse-IgG (LI-COR Biosciences, Inc. catalog # 926-68070) and donkey anti-rabbit-IgG (LI-COR Biosciences, Inc. catalog # 926-32213) IR-dye secondary antibodies for 1 h, washed three times with TBST and imaged using the LI-COR Odyssey CLx imager (LI-COR Biosciences, Inc.).

Immunostaining of *C. elegans* embryos and imaging

Immunostaining of *C. elegans* embryos was performed as described previously (O'Connell and Golden, 2014) with a few modifications. Briefly, gravid adults were dissected in 18 µl of M9 buffer to release embryos. The embryos were subjected to freeze cracking by flash-freezing the slides in liquid nitrogen and flicking off the glass coverslip placed on top of the embryos. The embryos were then fixed in 100% methanol prechilled to −30°C and blocked with 1× Tris-buffered saline with 5% bovine serum albumin and 0.5% Tween 20 (TBSBT). The embryos were incubated with rabbit anti-HA (1:1000; Cell Signaling Technology, catalog #3724S) and mouse anti-α-tubulin (1:200; Santa Cruz Biotechnology, catalog #sc-32293) antibodies for overnight at 4°C. The slides were washed three times with TBSBT and incubated with goat anti-mouse-IgG conjugated to Alexa Fluor 568 (Thermo Fisher Scientific Inc., Catalog #A-11004) and goat anti-rabbit-IgG conjugated to Alexa Fluor 488 (Thermo Fisher Scientific Inc., Waltham, MA; catalog #A-11034) secondary antibodies for 1 h at room temperature. The slides were then washed three times with TBSBT, and the embryos were mounted on glass coverslips using the Vectashield mounting medium containing DAPI (Vector Laboratories, Inc., Burlingame, CA; catalog # H-2000-10). The mounted slides were kept in the dark at room temperature overnight and the coverslips were sealed with nail polish 24 h later. The slides were then imaged using a Yokagawa spinning disk mounted on an Olympus confocal microscope with an *xyz* automated stage equipped with three laser lines (405 nm, 488 nm and 561 nm) (Olympus America, Inc., Waltham, MA).

C. elegans brood count assays and embryonic viability assays

All brood count assays were performed at 20°C. For brood counts, L4 stage *C. elegans* from each genotype were transferred onto 35 mm MYOB plates seeded with OP50 bacteria. Each L4 worm was transferred onto a single MYOB plate and the plate was numbered. The parent worm from each numbered plate was transferred to a new plate every 24 h until the parent stopped producing progeny. All the progeny produced by each of the parent worms were counted each day starting from Day 3 and the number of dead and live progeny were determined. For embryonic viability assays, the percentage of live progeny produced by each parent worm was quantified by dividing the number of live progeny produced by each worm by the total number of progeny produced by the same worm.

C. elegans body length measurements and vulva imaging

Differential interference contrast (DIC) live imaging was performed using a Nikon Eclipse fluorescence microscope (Nikon Instruments, Inc., Melville, NY) to measure *C. elegans* body length and to examine *C. elegans* vulva development. For these assays, gravid adult worms of each genotype were picked into 6 to 8 µl of M9 buffer with 1 mM levamisole. The worms were then mounted on a 2% agarose pad and imaged at either a 20× (body length measurement assays) or a 40× magnification (vulva development assays) using the Nikon NIS-Elements software (Nikon Instruments, Inc.). For *C. elegans* body length measurements, multiple images were taken for each worm at 20× magnification. The images were then aligned, overlapped and stitched together using the Adobe Photoshop software (Adobe Inc., Mountain View, CA). The stitched images were used to measure worm body length using the Nikon NIS-Elements software (Nikon Instruments, Inc.). Additional colored background was added outside the body length images without altering the stitched images for better presentation.

Journal of Cell Science (2022) 135, jcs259396. doi:10.1242/jcs.259396

Phasmid cilia imaging

Males from the PY6100 strain (*oyIs59 Is[osm-6p::gfp] III*) were crossed with hermaphrodites from the IYR021 strain (*vps-26(luv-21) IV*) to introduce GFP expressed from the *osm-6* promoter into the *vps-26*-knockout strain. This strain was named IYR025 (*oyIs59 Is[osm-6p::gfp] III; vps-26(luv21) IV)*. For phasmid cilia imaging, *C. elegans* at the L4 stage of development from both PY6100 (control) and IYR025 strains grown at a temperature of 15.3°C were transferred to 16°C overnight and phasmid cilia were imaged the next day. To image the phasmid cilia, four to six adults from each genotype were transferred onto a coverslip with 5.5 µl of 10 mM levamisole in M9 buffer for 5 to 7 min to anaesthetize the worms. Following this, the worms were mounted on a 2% agarose pad on a glass slide and the coverslips were sealed with Vaseline. The slides were imaged within 30 min of the worms being mounted on them imaged using a Olympus IX83 spinning disk confocal microscope coupled with a Yokogawa X1 Scan head (Olympus America Inc., Waltham, MA). All images were taken at the same laser intensity (30.01%) and at the same exposure time (500.04 ms). To image the cilia, *Z*-slices of 0.25 µm were taken from the top to the bottom of each phasmid cilium. *Z*-projections for each of these images were used for quantifying phasmid cilia length.

Phasmid cilia length quantification

Soluble GFP expressed from the *osm-6* promoter was used as a proxy for measuring cilia length in this assay. To measure phasmid cilia length, the *Z*-projections for each phasmid cilium were used. The CellSens imaging software (Olympus America Inc.) was used for computing the *Z*-projections and for measuring all the phasmid cilia lengths. For the longer phasmid cilia length measurements, the polyline tool was used to draw a line from the base of the basal body to the tip of the longer of the two phasmid cilia to measure the cilia length in pixels. The resulting cilia lengths were calculated using the formula cilia length in µm = (length in pixels × 110)/1000. For the shorter cilia measurements, only those images that clearly differentiated the longer phasmid cilium from the shorter phasmid cilium were used for the cilia length analysis. In this analysis, the polyline tool in the CellSens software was again used to measure the distance in pixels between the base of the basal body and the tip of the cilium and converted to µm as described earlier. However, in the shorter cilia length analysis, only the length of the shorter of the two phasmid cilia was analyzed and used for quantification.

Statistical analysis of *C. elegans* studies

For *C. elegans* brood size, embryonic viability, body length measurement and phasmid cilia length assays, the data obtained were used to generate graphs using the GraphPad Prism software (GraphPad Software, Inc., San Diego, CA). A two-tailed unpaired *t*-test was used to calculate the *P*-value for each assay to determine whether the observed differences between the two genotypes were statistically significant. Middle error bar represents the mean while the top and bottom error bars represent the standard deviation.

Reagents and antibodies for mammalian cell studies

For catalog number and dilutions, please see Table S3. Antibodies were purchased from suppliers as indicated: mouse monoclonal anti-acetylated-tubulin antibodies (Sigma-Aldrich, St. Louis, MO), rabbit polyclonal antibodies to anti-acetylated-tubulin (Cell Signaling Technology, Danvers, MA), rabbit polyclonal anti-CP110 antibodies (ProteinTech, Rosemont, IL), rabbit polyclonal anti-myosin Va antibodies (Novus Biologicals, Littleton, CO), mouse monoclonal anti-GFP antibodies (Sigma-Aldrich), mouse monoclonal anti-MICAL-L1 antibodies (Novus Biologicals), mouse monoclonal anti-glyceraldehyde 3-phosphate dehydrogenase (GAPDH) antibodies conjugated with HRP (ProteinTech), mouse monoclonal anti-actin antibodies (Novus Biologicals), rabbit polyclonal anti-SNX1 antibodies (Novus Biologicals), mouse monoclonal anti-SNX2 antibodies (BD Transduction laboratories, Franklin Lakes, NJ), rabbit monoclonal anti-SNX5 antibodies (Abcam, Cambridge, MA), rabbit polyclonal anti-VPS26 antibodies (Abcam), rabbit monoclonal anti-VPS35 antibodies (Abcam), rabbit polyclonal anti-VPS29 antibodies (Santa Cruz Biotechnology), mouse monoclonal anti-SNX27 antibodies (Abcam). All secondary antibodies used for immunofluorescence were purchased from Molecular Probes (Eugene, OR).

Cell culture, induction of ciliogenesis and siRNA knockdown

The human epithelial cell line hTERT RPE-1 (ATCC-CRL4000) was grown at 37°C in 5% CO_2 in Dulbecco's modified Eagle's medium with F12 (DMEM/F12; Thermo Fisher Scientific, Carlsbad, CA) containing 10% fetal bovine serum (FBS; Sigma-Aldrich), 2 mM L-glutamine, 100 U/ml penicillin/streptomycin and 1× non-essential amino acids (Thermo Fisher Scientific, Waltham, MA). The CRISPR/Cas9 gene-edited NIH3T3 cell line expressing endogenous levels of EHD1 with GFP attached to its C-terminus was generated as described previously (Yeow et al., 2017). Gene-edited NIH3T3 cells were cultured at 37°C in 5% CO_2 in DMEM (GE Healthcare, Chicago, IL) containing 10% FBS, with 2 mM L-glutamine and 100 U/ml penicillin/streptomycin. To induce ciliogenesis, RPE-1 cells were incubated in DMEM/F12 with 2 mM L-glutamine, 1× non-essential amino acids and 0.2% FBS for the indicated times (starvation medium). NIH3T3 cells were grown in serum-free DMEM with 2 mM L-glutamine for the indicated times. All cell lines are also routinely tested for *Mycoplasma*.

For siRNA knockdown, ∼5.0×10^4 RPE-1 or NIH3T3 cells were plated on coverslips in a 35 mm culture dish for 16 h, and then transfected with 200 nM of oligonucleotides using Lipofectamine RNAi/MAX (Invitrogen, Carlsbad, CA) for 72 h in the absence of antibiotics, or with Lipofectamine RNAi/MAX alone for mock-treated control cells, as per the manufacturer's protocol. Oligonucleotides targeting human VPS26a (5′-GCCUUACCUGGAGAACUGA[dT][dT]-3′), human VPS35 (5′-GGUGUAAAUGUGGAACGUU[dT][dT]-3′), human VPS29 (5′-AAGUUGUGACUGUUGGACA[dT][dT]-3′), human EHD1 (5′-CCAAUGUCUUUGGUAAAGA[dT][dT]-3′), human MICAL-L1 (5′-GACAAUGUCUUCGAGAAUA(dT)(dT)-3′), human SNX1 (5′-GACAUUGAGUGGUGCUGGU[dT][dT]-3′ and 5′-GACAUUUGGUUUGAGGAGA[dT][dT]-3′), human SNX2 (5′-GGAAGAUGCUCAAAUUACU[dT][dT]-3′ and 5′-CUUAGGAAACUUCAUGUCA[dT][dT]-3′), human SNX5 (5′-CAGUAAAGAUCGCAACUUU[dT][dT]-3′ and 5′-CGUUUCAGAGCCCAGAGUU[dT][dT]-3′), human SNX27 (5′-CUCUACAUUCAGAAUUAUA[dT][dT]-3′ and 5′-CUAAUGAGUUUCCUCACAA[dT][dT]-3′), mouse VPS26a (5′-CUAUUCCGAUAAGAUUGUU[dT][dT]-3′and 5′-GAAUUACAGCUGAUCAAGA[dT][dT]-3′), and mouse VPS35 (5′-GAUUCGAGAAGAUCUCCCA[dT][dT]-3′ and 5′-GUAAUGUUCUGGAUUAUAA[dT][dT]-3′) were purchased from Sigma-Aldrich. At 24 h after transfection, the culture medium was replaced with fresh starvation medium for ciliogenesis induction. The efficiency of knockdown was determined by immunoblotting.

Co-immunoprecipitation

hTERT RPE-1 cells growing in 100 mm dishes were lysed in lysis buffer containing 50 mM Tris-HCl pH 7.4, 150 mM NaCl, 1 mM $MgCl_2$, 1% Triton X-100 and freshly added protease inhibitor cocktail (Roche, Basel, Switzerland). Cell debris was eliminated by centrifugation at 1889 ***g*** at 4°C for 10 min. The cleared lysate was collected and incubated with anti-CP110 antibodies overnight at 4°C. Protein G-agarose beads (GE Healthcare) were added to the lysate–antibody mix and left to rock at 4°C for 2 h. Samples were then washed three times with washing buffer containing 50 mM Tris-HCl pH 7.4, 150 mM NaCl, 1 mM $MgCl_2$ and 0.1% Triton X-100. Protein complexes were eluted from the beads by boiling the sample for 10 min in the presence of 4× loading buffer containing 250 mM Tris-HCl pH 6.8, 8% SDS, 40% glycerol, 5% β-mercaptoethanol and 0.2% (w/v) Bromophenol Blue. Eluted proteins were detected by immunoblotting.

Immunoblotting of proteins from mammalian cells

Cells in culture were washed twice with pre-chilled PBS and harvested with a rubber cell scraper. Cell pellets were lysed by resuspending in lysis buffer containing 50 mM Tris-HCl pH 7.4, 150 mM NaCl, 1% NP-40, 0.5% sodium deoxycholate and freshly added protease inhibitor cocktail (Roche) for 30 min on ice. The cell lysates were then centrifuged at 1889 ***g*** at 4°C for 10 min. The concentration of protein from each sample was measured with Bio-Rad protein assay (Bio-Rad, Hercules, CA), equalized, and eluted by

boiling with 4× loading buffer. Proteins from either cell lysates or immunoprecipitations were separated by SDS-PAGE on 10% gels, and transferred onto nitrocellulose membranes (Midsci, St. Louis, MO). Membranes were blocked for 30 min at room temperature in PBS containing 0.3% (v/v) Tween-20 (PBST) and 5% dried milk, and then incubated overnight at 4°C with diluted primary antibodies (Table S3). Protein–antibody complexes were detected with HRP-conjugated goat anti-mouse-IgG (Jackson Research Laboratories, Bar Harbor, ME) or donkey anti-rabbit-IgG (GE Healthcare) secondary antibodies for 1 h at room temperature, followed by incubation with an enhanced chemiluminescence substrate (Thermo Fisher Scientific). Immunoblot images were acquired by iBright Imaging Systems (Invitrogen).

Immunofluorescence and microscopy imaging of mammalian cells

Cells plated on coverslips were fixed in 100% methanol at −20°C for 5 min, followed by three rinses with PBS buffer. For immunofluorescence staining, cells were first permeabilized in 0.5% Triton-X plus 0.5% BSA in PBS for 30 min, and then stained with appropriate primary antibodies diluted in PBS buffer containing 0.1% Triton-X and 0.5% BSA for 1 h at room temperature (Table S3). PBS washes were applied to remove unbound primary antibodies. Cells were then incubated with fluorochrome-conjugated secondary antibodies for 1 h at room temperature and washed three more times in PBS. Coverslips were mounted in Fluoromount G Mounting medium (SouthernBiotech). Imaging was performed with a Zeiss LSM 800 confocal microscope (Carl Zeiss, Oberkochen, Germany) using a Plan-Apochromat 63×/1.4 NA oil objective and appropriate filters, as previously described (Xie et al., 2016). Structured illumination microscopy (SIM) imaging was performed with a Zeiss ELYRA PS.1 illumination system (Carl Zeiss) using a 63× oil objective lens with NA of 1.4. Two lasers were used in the image acquisition: 568 nm, and 488 nm. Three orientation angles of the excitation grid were acquired for each *Z*-plane, with *Z* spacing of 110 nm between planes. Image acquisition and SIM processing was carried out with Zen software (Carl Zeiss). *Z*-slices were *z*-projected with ImageJ (National Institutes of Health, Bethesda, MD). Images were cropped, adjusted for brightness (whole-image adjustment) with minimal manipulation for better presentation. For quantification, three independent experiments were carried out, and the number of samples collected for quantification is described in the text.

Statistical analysis of mammalian cell experiments

Data obtained from ImageJ was exported to GraphPad Prism 6 (GraphPad, San Diego, CA). Bar graphs were created representing the mean and s.d. from data obtained from three independent experiments. Statistical significance was calculated with an unpaired two-tailed *t*-test.

Acknowledgements

The wild-type N2 strain was provided by the CGC, which is funded by NIH Office of Research Infrastructure Programs (P40 OD010440). The authors would like to thank Piali Sengupta (Brandeis University, Waltham, MA) for sending us the PY6100 pan-ciliary marker strain and Dr Ashish Maurya (Brandeis University, Waltham, MA) for helpful discussions regarding the phenotypes exhibited by the *vps-26*-knockout worms. We would also like to acknowledge Ms Erin Haastrup and Ms Rebecca Kitchen for their technical assistance.

Competing interests

The authors declare no competing or financial interests.

Author contributions

Conceptualization: S.X., N.N., J.I., S.C.; Methodology: S.X.; Validation: S.X., J.I., S.C.; Formal analysis: S.X., J.I., S.C.; Investigation: S.X., C.D., E.S., R.D., A.W., A.D., D.M., J.I., S.C.; Resources: J.I., S.C.; Data curation: S.X., J.I., S.C.; Writing - original draft: S.X., N.N., J.I., S.C.; Writing - review & editing: S.X., J.I., S.C.; Visualization: S.X., J.I., S.C.; Supervision: N.N., J.I., S.C.; Project administration: J.I., S.C.; Funding acquisition: N.N., J.I., S.C.

Funding

The authors acknowledge funding from the National Institute of General Medical Sciences (NIGMS) of the National Institutes of Health (NIH) for the following grant support [R01GM123557 and R01GM133915 to S.C., 5P20GM103636-09 to J.I.], TU Student Research Grants [E.S. and C.D.], TU Faculty Summer Development Fellowship [J.I.], TU Chemistry Summer Undergraduate Research Program [E.S., C.D., D.M., A.O.], Tulsa Undergraduate Research Challenge [E.S., C.D., D.M.], and TU start-up funds [J.I.]. Deposited in PMC for release after 12 months

Peer review history

The peer review history is available online at https://journals.biologists.com/jcs/article-lookup/doi/10.1242/jcs.259396.

References

Arighi, C. N., Hartnell, L. M., Aguilar, R. C., Haft, C. R. and Bonifacino, J. S. (2004). Role of the mammalian retromer in sorting of the cation-independent mannose 6-phosphate receptor. *J. Cell Biol.* **165**, 123-133. doi:10.1083/jcb.200312055

Bayer, E. A., Sun, H., Rafi, I. and Hobert, O. (2020). Temporal, spatial, sexual and environmental regulation of the master regulator of sexual differentiation in C. elegans. *Curr. Biol.* **30**, 3604-3616.e3. doi:10.1016/j.cub.2020.06.060

Braschi, E., Goyon, V., Zunino, R., Mohanty, A., Xu, L. and McBride, H. M. (2010). Vps35 mediates vesicle transport between the mitochondria and peroxisomes. *Curr. Biol.* **20**, 1310-1315. doi:10.1016/j.cub.2010.05.066

Bugarcic, A., Zhe, Y., Kerr, M. C., Griffin, J., Collins, B. M. and Teasdale, R. D. (2011). Vps26A and Vps26B subunits define distinct retromer complexes. *Traffic* **12**, 1759-1773. doi:10.1111/j.1600-0854.2011.01284.x

C. elegans Deletion Mutant Consortium. (2012). large-scale screening for targeted knockouts in the Caenorhabditis elegans genome. *G3 (Bethesda)* **2**, 1415-1425. doi:10.1534/g3.112.003830

Chen, D., Xiao, H., Zhang, K., Wang, B., Gao, Z., Jian, Y., Qi, X., Sun, J., Miao, L. and Yang, C. (2010). Retromer is required for apoptotic cell clearance by phagocytic receptor recycling. *Science* **327**, 1261-1264. doi:10.1126/science.1184840

Chen, K. E., Healy, M. D. and Collins, B. M. (2019). Towards a molecular understanding of endosomal trafficking by Retromer and Retriever. *Traffic* **20**, 465-478. doi:10.1111/tra.12649

Clairfeuille, T., Mas, C., Chan, A. S. M., Yang, Z., Tello-Lafoz, M., Chandra, M., Widagdo, J., Kerr, M. C., Paul, B., Mérida, I. et al. (2016). A molecular code for endosomal recycling of phosphorylated cargos by the SNX27-retromer complex. *Nat. Struct. Mol. Biol.* **23**, 921-932. doi:10.1038/nsmb.3290

Coudreuse, D. Y. M., Roël, G., Betist, M. C., Destrée, O. and Korswagen, H. C. (2006). Wnt gradient formation requires retromer function in Wnt-producing cells. *Science* **312**, 921-924. doi:10.1126/science.1124856

Cullen, P. J. and Korswagen, H. C. (2012). Sorting nexins provide diversity for retromer-dependent trafficking events. *Nat. Cell Biol.* **14**, 29-37. doi:10.1038/ncb2374

Dhawan, K., Naslavsky, N. and Caplan, S. (2020). Sorting nexin 17 (SNX17) links endosomal sorting to Eps15 homology domain protein 1 (EHD1)-mediated fission machinery. *J. Biol. Chem.* **295**, 3837-3850. doi:10.1074/jbc.RA119.011368

Donoso, M., Cancino, J., Lee, J., van Kerkhof, P., Retamal, C., Bu, G., Gonzalez, A., Cáceres, A. and Marzolo, M.-P. (2009). Polarized traffic of LRP1 involves AP1B and SNX17 operating on Y-dependent sorting motifs in different pathways. *Mol. Biol. Cell* **20**, 481-497. doi:10.1091/mbc.e08-08-0805

Evans, A. J., Daly, J. L., Anuar, A. N. K., Simonetti, B. and Cullen, P. J. (2020). Acute inactivation of retromer and ESCPE-1 leads to time-resolved defects in endosomal cargo sorting. *J. Cell Sci.* **133**, jcs246033. doi:10.1242/jcs.246033

Farfán, P., Lee, J., Larios, J., Sotelo, P., Bu, G. and Marzolo, M.-P. (2013). A sorting nexin 17-binding domain within the LRP1 cytoplasmic tail mediates receptor recycling through the basolateral sorting endosome. *Traffic* **14**, 823-838. doi:10.1111/tra.12076

Farmer, T., Reinecke, J. B., Xie, S., Bahl, K., Naslavsky, N. and Caplan, S. (2017). Control of mitochondrial homeostasis by endocytic regulatory proteins. *J. Cell Sci.* **130**, 2359-2370. doi:10.1242/jcs.204537

Farmer, T., Naslavsky, N. and Caplan, S. (2018). Tying trafficking to fusion and fission at the mighty mitochondria. *Traffic* **19**, 569-577. doi:10.1111/tra.12573

Farmer, T., O'Neill, K. L., Naslavsky, N., Luo, X. and Caplan, S. (2019). Retromer facilitates the localization of Bcl-xL to the mitochondrial outer membrane. *Mol. Biol. Cell* **30**, 1138-1146. doi:10.1091/mbc.E19-01-0044

Feng, S., Knödler, A., Ren, J., Zhang, J., Zhang, X., Hong, Y., Huang, S., Peränen, J. and Guo, W. (2012). A Rab8 guanine nucleotide exchange factor-effector interaction network regulates primary ciliogenesis. *J. Biol. Chem.* **287**, 15602-15609. doi:10.1074/jbc.M111.333245

Feng, S., Wu, B., Peränen, J. and Guo, W. (2015). Kinetic activation of Rab8 guanine nucleotide exchange factor Rabin8 by Rab11. *Methods Mol. Biol.* **1298**, 99-106. doi:10.1007/978-1-4939-2569-8_8

Follett, J., Norwood, S. J., Hamilton, N. A., Mohan, M., Kovtun, O., Tay, S., Zhe, Y., Wood, S. A., Mellick, G. D., Silburn, P. A. et al. (2014). The Vps35 D620N mutation linked to Parkinson's disease disrupts the cargo sorting function of retromer. *Traffic* **15**, 230-244. doi:10.1111/tra.12136

Fujiwara, M., Sengupta, P. and McIntire, S. L. (2002). Regulation of body size and behavioral state of C. elegans by sensory perception and the EGL-4 cGMP-

dependent protein kinase. *Neuron* **36**, 1091-1102. doi:10.1016/S0896-6273(02)01093-0

Gallon, M., Clairfeuille, T., Steinberg, F., Mas, C., Ghai, R., Sessions, R. B., Teasdale, R. D., Collins, B. M. and Cullen, P. J. (2014). A unique PDZ domain and arrestin-like fold interaction reveals mechanistic details of endocytic recycling by SNX27-retromer. *Proc. Natl. Acad. Sci. USA* **111**, E3604-E3613. doi:10.1073/pnas.1410552111

Gleason, R. J., Akintobi, A. M., Grant, B. D. and Padgett, R. W. (2014). BMP signaling requires retromer-dependent recycling of the type I receptor. *Proc. Natl. Acad. Sci. USA* **111**, 2578-2583. doi:10.1073/pnas.1319947111

Gleason, R. J., Vora, M., Li, Y., Kane, N. S., Liao, K. and Padgett, R. W. (2017). C. elegans SMA-10 regulates BMP receptor trafficking. *PLoS ONE* **12**, e0180681. doi:10.1371/journal.pone.0180681

Gokool, S., Tattersall, D. and Seaman, M. N. J. (2007). EHD1 interacts with retromer to stabilize SNX1 tubules and facilitate endosome-to-Golgi retrieval. *Traffic* **8**, 1873-1886. doi:10.1111/j.1600-0854.2007.00652.x

Gomez, T. S. and Billadeau, D. D. (2009). A FAM21-containing WASH complex regulates retromer-dependent sorting. *Dev. Cell* **17**, 699-711. doi:10.1016/j.devcel.2009.09.009

Goncalves, A. B., Hasselbalch, S. K., Joensen, B. B., Patzke, S., Martens, P., Ohlsen, S. K., Quinodoz, M., Nikopoulos, K., Suleiman, R., Damso Jeppesen, M. P. et al. (2021). CEP78 functions downstream of CEP350 to control biogenesis of primary cilia by negatively regulating CP110 levels. *eLife* **10**, e63731. doi:10.7554/eLife.63731.sa2

Griffin, C. T., Trejo, J. A. and Magnuson, T. (2005). Genetic evidence for a mammalian retromer complex containing sorting nexins 1 and 2. *Proc. Natl. Acad. Sci. USA* **102**, 15173-15177. doi:10.1073/pnas.0409558102

Haft, C. R., de la Luz Sierra, M., Bafford, R., Lesniak, M. A., Barr, V. A. and Taylor, S. I. (2000). Human orthologs of yeast vacuolar protein sorting proteins Vps26, 29, and 35: assembly into multimeric complexes. *Mol. Biol. Cell* **11**, 4105-4116. doi:10.1091/mbc.11.12.4105

Hagemann, N., Ackermann, N., Christmann, J., Brier, S., Yu, F. and Erdmann, K. S. (2013). The serologically defined colon cancer antigen-3 interacts with the protein tyrosine phosphatase PTPN13 and is involved in the regulation of cytokinesis. *Oncogene* **32**, 4602-4613. doi:10.1038/onc.2012.485

Harbour, M. E., Breusegem, S. Y. A., Antrobus, R., Freeman, C., Reid, E. and Seaman, M. N. (2010). The cargo-selective retromer complex is a recruiting hub for protein complexes that regulate endosomal tubule dynamics. *J. Cell Sci.* **123**, 3703-3717. doi:10.1242/jcs.071472

Harterink, M., Port, F., Lorenowicz, M. J., McGough, I. J., Silhankova, M., Betist, M. C., van Weering, J. R. T., van Heesbeen, R. G. H. P., Middelkoop, T. C., Basler, K. et al. (2011). A SNX3-dependent retromer pathway mediates retrograde transport of the Wnt sorting receptor Wntless and is required for Wnt secretion. *Nat. Cell Biol.* **13**, 914-923. doi:10.1038/ncb2281

Hossain, D., Javadi Esfehani, Y., Das, A. and Tsang, W. Y. (2017). Cep78 controls centrosome homeostasis by inhibiting EDD-DYRK2-DDB1(Vpr)(BP). *EMBO Rep.* **18**, 632-644. doi:10.15252/embr.201642377

Iyer, J., DeVaul, N., Hansen, T. and Nebenfuehr, B. (2019). Using microinjection to generate genetically modified Caenorhabditis elegans by CRISPR/Cas9 editing. *Methods Mol. Biol.* **1874**, 431-457. doi:10.1007/978-1-4939-8831-0_25

Kerr, M. C., Bennetts, J. S., Simpson, F., Thomas, E. C., Flegg, C., Gleeson, P. A., Wicking, C. and Teasdale, R. D. (2005). A novel mammalian retromer component, Vps26B. *Traffic* **6**, 991-1001. doi:10.1111/j.1600-0854.2005.00328.x

Knödler, A., Feng, S., Zhang, J., Zhang, X., Das, A., Peränen, J. and Guo, W. (2010). Coordination of Rab8 and Rab11 in primary ciliogenesis. *Proc. Natl. Acad. Sci. USA* **107**, 6346-6351. doi:10.1073/pnas.1002401107

Kobayashi, T., Tsang, W. Y., Li, J., Lane, W. and Dynlacht, B. D. (2011). Centriolar kinesin Kif24 interacts with CP110 to remodel microtubules and regulate ciliogenesis. *Cell* **145**, 914-925. doi:10.1016/j.cell.2011.04.028

Kovtun, O., Leneva, N., Bykov, Y. S., Ariotti, N., Teasdale, R. D., Schaffer, M., Engel, B. D., Owen, D. J., Briggs, J. A. G. and Collins, B. M. (2018). Structure of the membrane-assembled retromer coat determined by cryo-electron tomography. *Nature* **561**, 561-564.

Kumar, K. R., Weissbach, A., Heldmann, M., Kasten, M., Tunc, S., Sue, C. M., Svetel, M., Kostic, V. S., Segura-Aguilar, J., Ramirez, A. et al. (2012). Frequency of the D620N mutation in VPS35 in Parkinson disease. *Arch. Neurol.* **69**, 1360-1364. doi:10.1001/archneurol.2011.3367

Kvainickas, A., Jimenez-Orgaz, A., Nagele, H., Hu, Z., Dengjel, J. and Steinberg, F. (2017). Cargo-selective SNX-BAR proteins mediate retromer trimer independent retrograde transport. *J. Cell Biol.* **216**, 3677-3693. doi:10.1083/jcb.201702137

Kvainickas, A., Nägele, H., Qi, W., Dokládal, L., Jimenez-Orgaz, A., Stehl, L., Gangurde, D., Zhao, Q., Hu, Z., Dengjel, J. et al. (2019). Retromer and TBC1D5 maintain late endosomal RAB7 domains to enable amino acid-induced mTORC1 signaling. *J. Cell Biol.* **218**, 3019-3038. doi:10.1083/jcb.201812110

Lauffer, B. E. L., Melero, C., Temkin, P., Lei, C., Hong, W., Kortemme, T. and von Zastrow, M. (2010). SNX27 mediates PDZ-directed sorting from endosomes to the plasma membrane. *J. Cell Biol.* **190**, 565-574. doi:10.1083/jcb.201004060

Lee, T. Y., Yoon, K.-H. and Lee, J. I. (2016). NGT-3D: a simple nematode cultivation system to study Caenorhabditis elegans biology in 3D. *Biol. Open* **5**, 529-534. doi:10.1242/bio.015743

Leneva, N., Kovtun, O., Morado, D. R., Briggs, J. A. G. and Owen, D. J. (2021). Architecture and mechanism of metazoan retromer:SNX3 tubular coat assembly. *Sci. Adv.* **7**, eabf8598. doi:10.1126/sciadv.abf8598

Lo, C.-H., Lin, I.-H., Yang, T. T., Huang, Y.-C., Tanos, B. E., Chou, P.-C., Chang, C.-W., Tsay, Y.-G., Liao, J.-C. and Wang, W.-J. (2019). Phosphorylation of CEP83 by TTBK2 is necessary for cilia initiation. *J. Cell Biol.* **218**, 3489-3505. doi:10.1083/jcb.201811142

Lu, Q., Insinna, C., Ott, C., Stauffer, J., Pintado, P. A., Rahajeng, J., Baxa, U., Walia, V., Cuenca, A., Hwang, Y.-S. et al. (2015). Early steps in primary cilium assembly require EHD1/EHD3-dependent ciliary vesicle formation. *Nat. Cell Biol.* **17**, 531. doi:10.1038/ncb3155

Lucas, M., Gershlick, D. C., Vidaurrazaga, A., Rojas, A. L., Bonifacino, J. S. and Hierro, A. (2016). Structural mechanism for cargo recognition by the retromer complex. *Cell* **167**, 1623-1635.e14. doi:10.1016/j.cell.2016.10.056

Martinez-Velazquez, L. A. and Ringstad, N. (2018). Antagonistic regulation of trafficking to Caenorhabditis elegans sensory cilia by a Retinal Degeneration 3 homolog and retromer. *Proc. Natl. Acad. Sci. USA* **115**, E438-E447. doi:10.1073/pnas.1712302115

McGough, I. J., Steinberg, F., Gallon, M., Yatsu, A., Ohbayashi, N., Heesom, K. J., Fukuda, M. and Cullen, P. J. (2014). Identification of molecular heterogeneity in SNX27-retromer-mediated endosome-to-plasma-membrane recycling. *J. Cell Sci.* **127**, 4940-4953. doi:10.1242/jcs.156299

McKenzie, J. E., Raisley, B., Zhou, X., Naslavsky, N., Taguchi, T., Caplan, S. and Sheff, D. (2012). Retromer guides STxB and CD8-M6PR from early to recycling endosomes, EHD1 guides STxB from recycling endosome to Golgi. *Traffic* **13**, 1140-1159. doi:10.1111/j.1600-0854.2012.01374.x

McNally, K. E. and Cullen, P. J. (2018). Endosomal retrieval of cargo: retromer is not alone. *Trends Cell Biol.* **28**, 807-822. doi:10.1016/j.tcb.2018.06.005

McNally, K. E., Faulkner, R., Steinberg, F., Gallon, M., Ghai, R., Pim, D., Langton, P., Pearson, N., Danson, C. M., Nägele, H. et al. (2017). Retriever is a multiprotein complex for retromer-independent endosomal cargo recycling. *Nat. Cell Biol.* **19**, 1214-1225. doi:10.1038/ncb3610

Naslavsky, N. and Caplan, S. (2018). The enigmatic endosome - sorting the ins and outs of endocytic trafficking. *J. Cell Sci.* **131**, jcs216499. doi:10.1242/jcs.216499

Naslavsky, N. and Caplan, S. (2020). Endocytic membrane trafficking in the control of centrosome function. *Curr. Opin. Cell Biol.* **65**, 150-155. doi:10.1016/j.ceb.2020.01.009

Norwood, S. J., Shaw, D. J., Cowieson, N. P., Owen, D. J., Teasdale, R. D. and Collins, B. M. (2011). Assembly and solution structure of the core retromer protein complex. *Traffic* **12**, 56-71. doi:10.1111/j.1600-0854.2010.01124.x

O'Connell, K. F. and Golden, A. (2014). Confocal imaging of the microtubule cytoskeleton in C. elegans embryos and germ cells. *Methods Mol. Biol.* **1075**, 257-272. doi:10.1007/978-1-60761-847-8_13

Patel, D., Xu, C., Nagarajan, S., Liu, Z., Hemphill, W. O., Shi, R., Uversky, V. N., Caldwell, G. A., Caldwell, K. A. and Witt, S. N. (2018). Alpha-synuclein inhibits Snx3-retromer-mediated retrograde recycling of iron transporters in S. cerevisiae and C. elegans models of Parkinson's disease. *Hum. Mol. Genet.* **27**, 1514-1532. doi:10.1093/hmg/ddy059

Prasad, B. C. and Clark, S. G. (2006). Wnt signaling establishes anteroposterior neuronal polarity and requires retromer in C. elegans. *Development* **133**, 1757-1766. doi:10.1242/dev.02357

Reddy, J. V. and Seaman, M. N. J. (2001). Vps26p, a component of retromer, directs the interactions of Vps35p in endosome-to-Golgi retrieval. *Mol. Biol. Cell* **12**, 3242-3256. doi:10.1091/mbc.12.10.3242

Rojas, R., Kametaka, S., Haft, C. R. and Bonifacino, J. S. (2007). Interchangeable but essential functions of SNX1 and SNX2 in the association of retromer with endosomes and the trafficking of mannose 6-phosphate receptors. *Mol. Cell. Biol.* **27**, 1112-1124. doi:10.1128/MCB.00156-06

Schmid, T. and Hajnal, A. (2015). Signal transduction during C. elegans vulval development: a NeverEnding story. *Curr. Opin. Genet. Dev.* **32**, 1-9. doi:10.1016/j.gde.2015.01.006

Schouteden, C., Serwas, D., Palfy, M. and Dammermann, A. (2015). The ciliary transition zone functions in cell adhesion but is dispensable for axoneme assembly in C. elegans. *J. Cell Biol.* **210**, 35-44. doi:10.1083/jcb.201501013

Seaman, M. N. J. (2004). Cargo-selective endosomal sorting for retrieval to the Golgi requires retromer. *J. Cell Biol.* **165**, 111-122. doi:10.1083/jcb.200312034

Seaman, M. N. J. (2021). The retromer complex: from genesis to revelations. *Trends Biochem. Sci.* **46**, 608-620. doi:10.1016/j.tibs.2020.12.009

Seaman, M. N. J. and Williams, H. P. (2002). Identification of the functional domains of yeast sorting nexins Vps5p and Vps17p. *Mol. Biol. Cell* **13**, 2826-2840. doi:10.1091/mbc.02-05-0064

Seaman, M. N. J., Marcusson, E. G., Cereghino, J. L. and Emr, S. D. (1997). Endosome to Golgi retrieval of the vacuolar protein sorting receptor, Vps10p, requires the function of the VPS29, VPS30, and VPS35 gene products. *J. Cell Biol.* **137**, 79-92. doi:10.1083/jcb.137.1.79

Seaman, M. N. J., McCaffery, J. M. and Emr, S. D. (1998). A membrane coat complex essential for endosome-to-Golgi retrograde transport in yeast. *J. Cell Biol.* **142**, 665-681. doi:10.1083/jcb.142.3.665

Simonetti, B., Danson, C. M., Heesom, K. J. and Cullen, P. J. (2017). Sequence-dependent cargo recognition by SNX-BARs mediates retromer-independent transport of CI-MPR. *J. Cell Biol.* **216**, 3695-3712. doi:10.1083/jcb.201703015

Simonetti, B., Paul, B., Chaudhari, K., Weeratunga, S., Steinberg, F., Gorla, M., Heesom, K. J., Bashaw, G. J., Collins, B. M. and Cullen, P. J. (2019). Molecular identification of a BAR domain-containing coat complex for endosomal recycling of transmembrane proteins. *Nat. Cell Biol.* **21**, 1219-1233. doi:10.1038/s41556-019-0393-3

Smith, A., Bergwell, M., Smith, E., Mathew, D. and Iyer, J. (2020). CRISPR/Cas9 editing of the C. elegans rbm-3.2 gene using the dpy-10 Co-CRISPR screening marker and assembled ribonucleoprotein complexes. *J. Vis. Exp.* **166**, 62001. doi:10.3791/62001

Spektor, A., Tsang, W. Y., Khoo, D. and Dynlacht, B. D. (2007). Cep97 and CP110 suppress a cilia assembly program. *Cell* **130**, 678-690. doi:10.1016/j.cell.2007.06.027

Steinberg, F., Heesom, K. J., Bass, M. D. and Cullen, P. J. (2012). SNX17 protects integrins from degradation by sorting between lysosomal and recycling pathways. *J. Cell Biol.* **197**, 219-230. doi:10.1083/jcb.201111121

Steinberg, F., Gallon, M., Winfield, M., Thomas, E. C., Bell, A. J., Heesom, K. J., Tavare, J. M. and Cullen, P. J. (2013). A global analysis of SNX27-retromer assembly and cargo specificity reveals a function in glucose and metal ion transport. *Nat. Cell Biol.* **15**, 461-471. doi:10.1038/ncb2721

Stockinger, W., Sailler, B., Strasser, V., Recheis, B., Fasching, D., Kahr, L., Schneider, W. J. and Nimpf, J. (2002). The PX-domain protein SNX17 interacts with members of the LDL receptor family and modulates endocytosis of the LDL receptor. *EMBO J.* **21**, 4259-4267. doi:10.1093/emboj/cdf435

Strochlic, T. I., Setty, T. G., Sitaram, A. and Burd, C. G. (2007). Grd19/Snx3p functions as a cargo-specific adapter for retromer-dependent endocytic recycling. *J. Cell Biol.* **177**, 115-125. doi:10.1083/jcb.200609161

Temkin, P., Lauffer, B., Jäger, S., Cimermancic, P., Krogan, N. J. and von Zastrow, M. (2011). SNX27 mediates retromer tubule entry and endosome-to-plasma membrane trafficking of signalling receptors. *Nat. Cell Biol.* **13**, 715-721. doi:10.1038/ncb2252

Tilley, F. C., Gallon, M., Luo, C., Danson, C. M., Zhou, J. and Cullen, P. J. (2018). Retromer associates with the cytoplasmic amino-terminus of polycystin-2. *J. Cell Sci.* **131**, jcs211342. doi:10.1242/jcs.211342

van Kerkhof, P., Lee, J., McCormick, L., Tetrault, E., Lu, W., Schoenfish, M., Oorschot, V., Strous, G. J., Klumperman, J. and Bu, G. (2005). Sorting nexin 17 facilitates LRP recycling in the early endosome. *EMBO J.* **24**, 2851-2861. doi:10.1038/sj.emboj.7600756

Vieira, N., Bessa, C., Rodrigues, A. J., Marques, P., Chan, F.-Y., de Carvalho, A. X., Correia-Neves, M. and Sousa, N. (2018). Sorting nexin 3 mutation impairs development and neuronal function in Caenorhabditis elegans. *Cell. Mol. Life Sci.* **75**, 2027-2044. doi:10.1007/s00018-017-2719-2

Vilariño-Güell, C., Wider, C., Ross, O. A., Dachsel, J. C., Kachergus, J. M., Lincoln, S. J., Soto-Ortolaza, A. I., Cobb, S. A., Wilhoite, G. J., Bacon, J. A. et al. (2011). VPS35 mutations in Parkinson disease. *Am. J. Hum. Genet.* **89**, 162-167. doi:10.1016/j.ajhg.2011.06.001

Walsh, R. B., Dresselhaus, E. C., Becalska, A. N., Zunitch, M. J., Blanchette, C. R., Scalera, A. L., Lemos, T., Lee, S. M., Apiki, J., Wang, S. et al. (2021). Opposing functions for retromer and Rab11 in extracellular vesicle traffic at presynaptic terminals. *J. Cell Biol.* **220**, e202012034. doi:10.1083/jcb.202012034

Wang, W., Ma, X., Zhou, L., Liu, J. and Zhu, X. (2017). A conserved retromer sorting motif is essential for mitochondrial DLP1 recycling by VPS35 in Parkinson's disease model. *Hum. Mol. Genet.* **26**, 781-789. doi:10.1093/hmg/ddw430

Wang, J., Fedoseienko, A., Chen, B., Burstein, E., Jia, D. and Billadeau, D. D. (2018). Endosomal receptor trafficking: retromer and beyond. *Traffic* **19**, 578-590. doi:10.1111/tra.12574

Wang, P., Xia, J., Zhang, L., Zhao, S., Li, S., Wang, H., Cheng, S., Li, H., Yin, W., Pei, D. et al. (2019). SNX17 recruits USP9X to antagonize MIB1-mediated ubiquitination and degradation of PCM1 during serum-starvation-induced ciliogenesis. *Cells* **8**, 1335. doi:10.3390/cells8111335

Xie, S., Bahl, K., Reinecke, J. B., Hammond, G. R. V., Naslavsky, N. and Caplan, S. (2016). The endocytic recycling compartment maintains cargo segregation acquired upon exit from the sorting endosome. *Mol. Biol. Cell* **27**, 108-126. doi:10.1091/mbc.E15-07-0514

Xie, S., Reinecke, J. B., Farmer, T., Bahl, K., Yeow, I., Nichols, B. J., McLamarrah, T. A., Naslavsky, N., Rogers, G. C. and Caplan, S. (2018). Vesicular trafficking plays a role in centriole disengagement and duplication. *Mol. Biol. Cell* **29**, 2622-2631. doi:10.1091/mbc.E18-04-0241

Xie, S., Farmer, T., Naslavsky, N. and Caplan, S. (2019). MICAL-L1 coordinates ciliogenesis by recruiting EHD1 to the primary cilium. *J. Cell Sci.* **132**, jcs233973. doi:10.1242/jcs.233973

Ye, H., Ojelade, S. A., Li-Kroeger, D., Zuo, Z., Wang, L., Li, Y., Gu, J. Y., Tepass, U., Rodal, A. A., Bellen, H. J. et al. (2020). Retromer subunit, VPS29, regulates synaptic transmission and is required for endolysosomal function in the aging brain. *eLife* **9**, e51977. doi:10.7554/eLife.51977

Yeow, I., Howard, G., Chadwick, J., Mendoza-Topaz, C., Hansen, C. G., Nichols, B. J. and Shvets, E. (2017). EHD proteins cooperate to generate caveolar clusters and to maintain caveolae during repeated mechanical stress. *Curr. Biol.* **27**, 2951-2962.e5. doi:10.1016/j.cub.2017.07.047

Yu, F., Sharma, S., Skowronek, A. and Erdmann, K. S. (2016). The serologically defined colon cancer antigen-3 (SDCCAG3) is involved in the regulation of ciliogenesis. *Sci. Rep.* **6**, 35399. doi:10.1038/srep35399

Zhang, D., Isack, N. R., Glodowski, D. R., Liu, J., Chen, C. C.-H., Xu, X. Z. S., Grant, B. D. and Rongo, C. (2012a). RAB-6.2 and the retromer regulate glutamate receptor recycling through a retrograde pathway. *J. Cell Biol.* **196**, 85-101. doi:10.1083/jcb.201104141

Zhang, J., Naslavsky, N. and Caplan, S. (2012b). EHDs meet the retromer: complex regulation of retrograde transport. *Cell Logist.* **2**, 161-165. doi:10.4161/cl.20582

Zhang, J., Reiling, C., Reinecke, J. B., Prislan, I., Marky, L. A., Sorgen, P. L., Naslavsky, N. and Caplan, S. (2012c). Rabankyrin-5 interacts with EHD1 and Vps26 to regulate endocytic trafficking and retromer function. *Traffic* **13**, 745-757. doi:10.1111/j.1600-0854.2012.01334.x

Zimprich, A., Benet-Pagès, A., Struhal, W., Graf, E., Eck, S. H., Offman, M. N., Haubenberger, D., Spielberger, S., Schulte, E. C., Lichtner, P. et al. (2011). A mutation in VPS35, encoding a subunit of the retromer complex, causes late-onset Parkinson disease. *Am. J. Hum. Genet.* **89**, 168-175. doi:10.1016/j.ajhg.2011.06.008

Supplemental Fig. 1

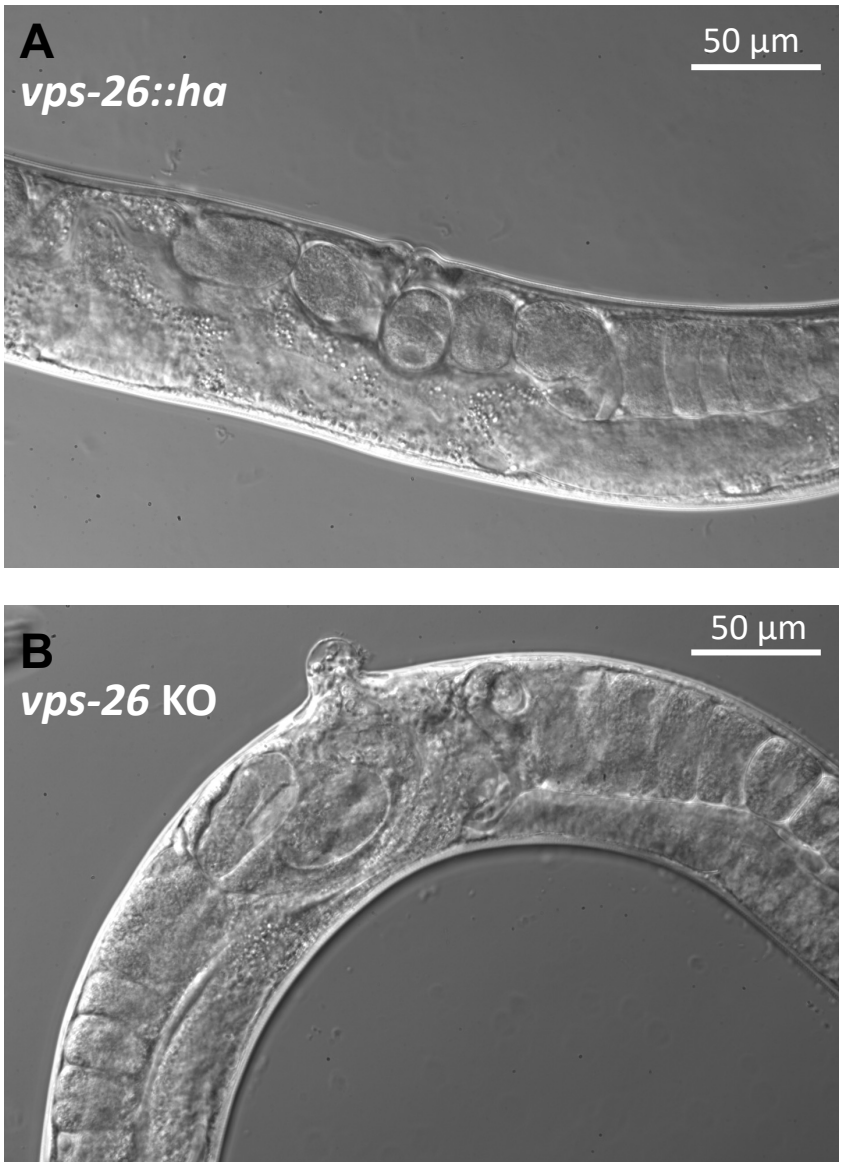

Fig. S1. Effect of *vps-26* knockout on vulva development in adult worms. (A) A representative DIC image of a normal adult *vps-26::ha* vulva. (B) A representative DIC image of an abnormal protruding vulva that is often seen in *vps-26* knockout worms.

Supplemental Fig. 2

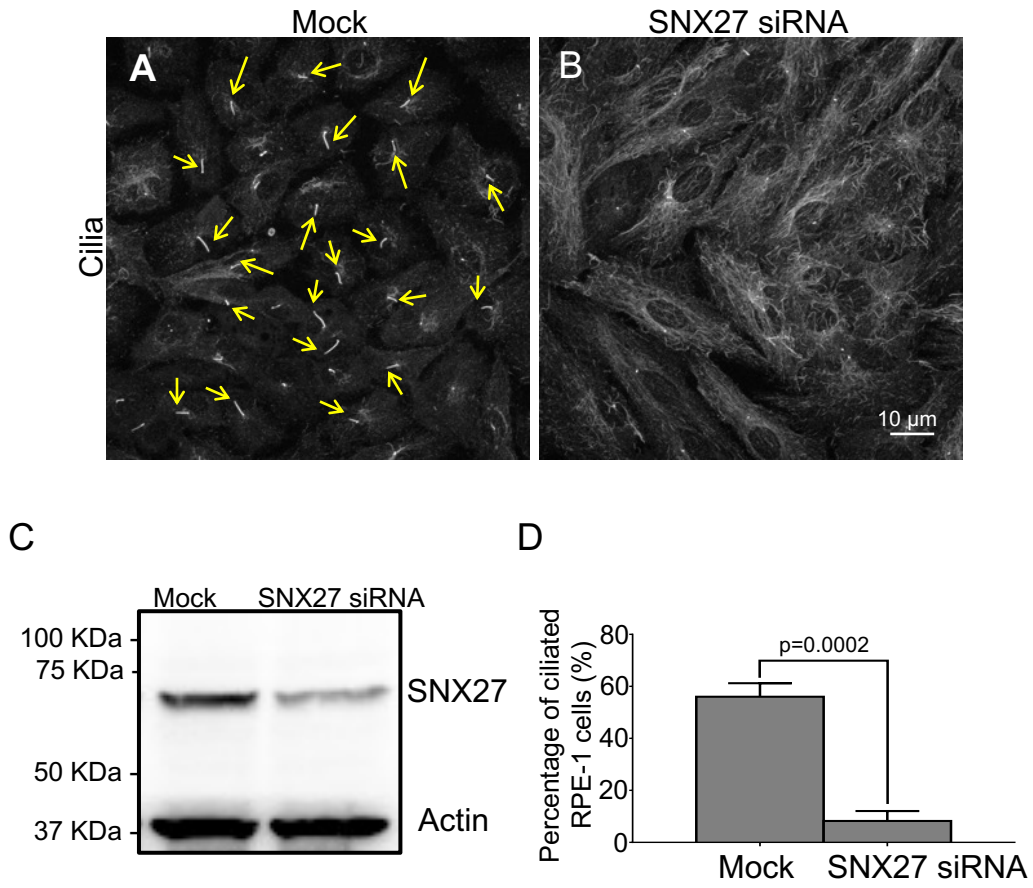

Fig. S2. SNX27 is required for normal ciliogenesis. (A-D) RPE-1 cells were Mock-treated (A) or SNX27-siRNA-treated (B) for 48 h, and serum-starved for 24 h to induce ciliogenesis. Cells were then fixed and immunostained with acetylated-tubulin to identify cilia/centrioles. Compared to Mock-treated cells (A), fewer cilia were generated upon depletion of SNX27 (B). (C) SNX27 siRNA-depletion efficacy was determined by immunoblotting. (D) The percentages of ciliated RPE-1 cells from either Mock- or siRNA-treated cover-slips were quantified and presented as a bar graph. The p-value was calculated for comparison between Mock- and siRNA-treated cells; n=3 experiments (>100 cells quantified for each experiment). Error bars denote standard deviation.

Supplemental Fig. 3

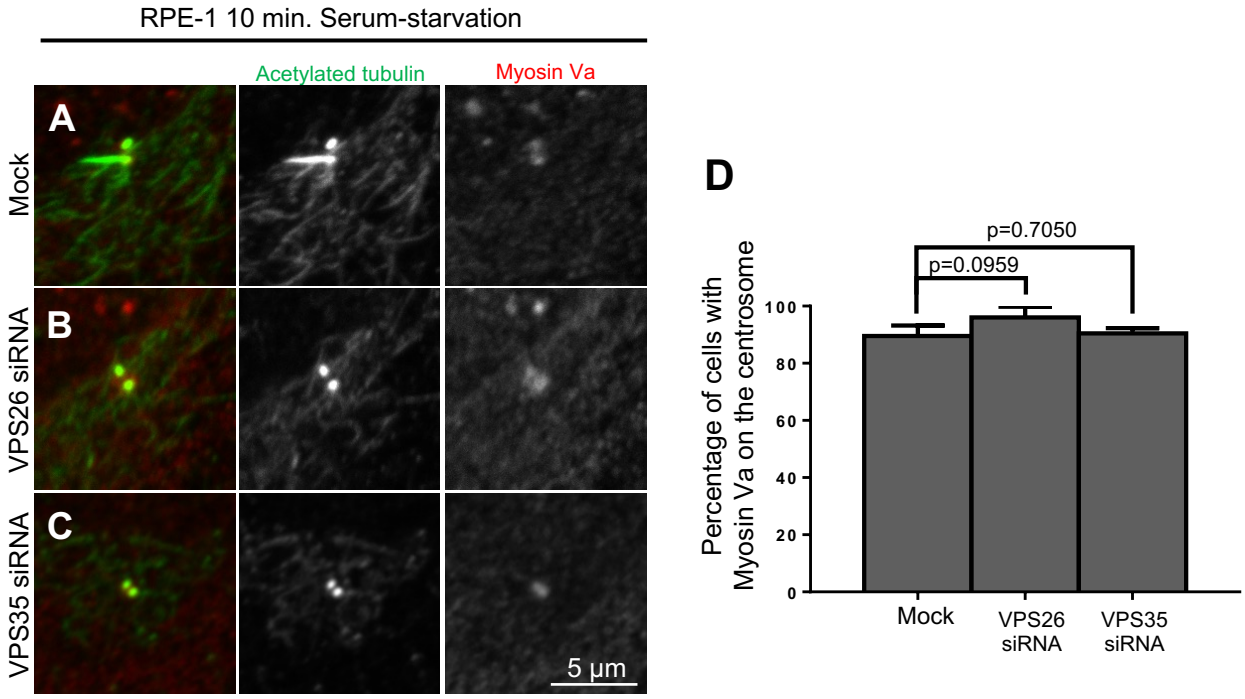

Fig. S3. Recruitment of preciliary vesicles to the centrosome is independent of the retromer. (A-D) RPE-1 cells were Mock-treated (A), VPS26-siRNA-treated (B), or VPS35-siRNA-treated (C), and serum-starved for 10 min to induce ciliogenesis. Immunoblots demonstrating siRNA depletion of these proteins is shown in Fig. 6. Cells were then fixed and immunostained with antibodies to acetylated-tubulin (green) to identify cilia/centrioles and Myosin Va (red) to mark preciliary vesicles. Myosin Va was detected on the centrosome in (A) Mock-treated, (B) VPS26-depleted and (C) VPS35-depleted cells. (D) The bar graph indicates the percentage of cells showing recruitment of Myosin Va onto cilia/centrioles. n=3 experiments (>100 cells quantified for each experiment). Error bars denote standard deviation.

Supplemental Fig. 4

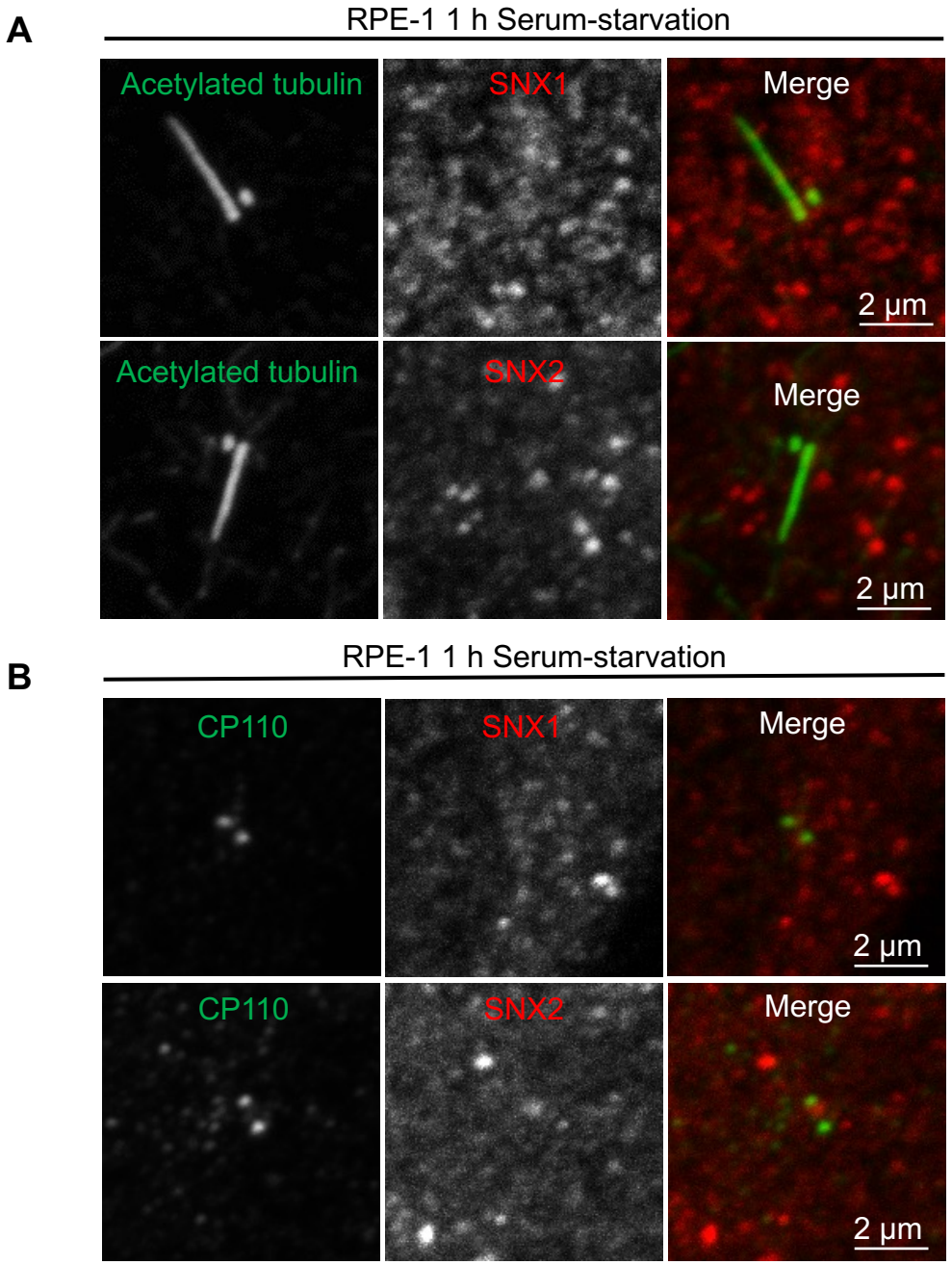

Fig. S4. SNX1 and SNX2 display minimal co-localization with cilia/basal bodies or CP110. (A) RPE-1 cells were fixed and immunostained using anti-acetylated-tubulin antibodies (green) and anti-SNX1 or anti-SNX2 antibodies (red). (B) RPE-1 cells were fixed and immunostained using anti-CP110 antibodies (green) and anti-SNX1 or anti-SNX2 antibodies (red). Immunofluorescence images were obtained by confocal microscopy. (C-D) Lack of CP110 co-immunoprecipitation with SNX1 and SNX2. RPE-1 cell lysates were subjected to immunoblotting (Input) or immunoprecipitation using anti-CP110 antibodies or rabbit anti-GFP antibodies (negative control). Immunoprecipitated proteins were immunoblotted with anti-CP110 (C and D), anti-SNX1 (C), and anti-SNX2 antibodies (D).

Table S1.

STRAIN	GENOTYPE	METHOD	RESOURCE
N2	WT	N/A	CGC
IYR010	*vps-26(luv10[vps-26::ha]) IV*	CRISPR	This study
IYR021	*vps-26(luv21) IV*	CRISPR	This study
PY6100	*oyIs59 Is[osm-6p::gfp] III*	N/A	Piali Sengupta Lab
IYR025	*oyIs59 Is[osm-6p::gfp] III; vps-26(luv21) IV*	Crossing	This study

Table S2.

Gene	Type of oligo	Sequence (5' to 3')
dpy-10 (Paix et al, 2015)	co-CRISPR crRNA	GCUACCAUAGGCACCACGAG
vps-26	KO crRNA#1	ACAAUAAAUUUCACAUUUAC
vps-26	KO crRNA#2	AUGGCGAUGCUUUUCGGCUU
vps-26	C-terminal HA-tag crRNA	GAAGAAUCAGAAUUAUCGUC
dpy-10 (Arribere et al, 2014)	*dyp-10(cn64)* repair oligo	CACTTGAACTTCAATACGGC
		AAGATGAGAATGACTGGAAA
		CCGTACCGCATGCGGTGCCTA
		TGGTAGCGGAGCTTCACATGG
		CTTCAGACCAACAGCCTAT
vps-26	KO repair oligo	GTTTATTTTCTGGAAAATAA
		ACAATAAATTTCACATTTAC
		TAAGTAGCCAATCAGCAGAA
		ATTCAAATTCGGCTCTCAAAT
		GAGGAT
vps-26	HA repair oligo	AATCGCCAAGATCGGATCCA
		AAAAGTGGATCAACAAGTCC
		TGATGACAACAGTGACAGTA
		GTTACCCATATGATGTTCCAG
		ATTACGCTTAGAGATAGAGAT

		AGTATTTCGATGCAATTAAAT
		CATTTT
vps-26	KO screening primer 1	CCTTGGGATGAAGCAGTTCC
vps-26	KO screening primer 2	TCCAGTAACTGATTCTCCATC
vps-26	HA screening primer 1	GGAAGTAACTCTCTGGCGAA
vps-26	HA screening primer 2	GAGAAACAAAACAAACGGGG

Table S3.

Antibodies	Host	Manufacturer	Catalogue#	Application	Dilution
Acetylated-tubulin	Mouse	Sigma	T7451	IF	1:100
Acetylated-tubulin	Rabbit	Cell signaling	5335	IF	1:100
Alpha tubulin	Mouse	Santa Cruz Biotechnology	sc-32293	IB, IF	1:200
CP110	Rabbit	Protein Tech	12794-1-AP	IF, IB,IP	1:200 (IF) 1:2000(IB)
Myosin Va	Rabbit	Novus	NBP1-92156	IF	1:500
GFP	Mouse	Roche	1184460001	IF	1:200
GFP	Rabbit	Pierce	PA1-980-A	IP	
HA	Rabbit	Cell Signaling	3724S	IB, IF	1:1000
Actin	Mouse	Novus	NB600-535	IB	1:5000
MICAL-L1	Mouse	Novus	H00085377-B01P	IF	1:200
MICAL-L1	Rabbit	LifeTein	RB1794	IB	1:1000
GAPDH-HRP	Mouse	Protein Tech	HRP60004	IB	1:2000
VPS26	Rabbit	Abcam	Ab23892	IB	1:1000
VPS35	Rabbit	Abcam	Ab157220	IF,IB	1:200 (IF) 1:1000 (IB)
SNX1	Rabbit	Novus	NBP2-13359	IF, IB	1:200 (IF) 1:500
SNX2	mouse	BD Transduction Laboratories	611308	IF, IB	1:200 (IF) 1:500
SNX5	Rabbit	Abcam	Ab180520	IB	1:500
SNX27	Mouse	Abcam	Ab77799	IB	1:800
Mouse HRP light chain only	Goat	Jackson	115-035-174	IB	1:7000
Rabbit HRP	Donkey			IB	1:5000
Mouse IRDye 680 RD	Goat	LI-COR	926-68070	IB	1:14000
Rabbit IRDye 800CW	Donkey	LI-COR	926-32213	IB	1:14000

Mouse Alexa 488	**Goat**	**Molecular Probe**	**A11029**	**IF**	**1:500**
Rabbit Alexa 568	**Goat**	**Molecular Probe**	**A11036**	**IF**	**1:500**
Mouse Alexa 568	**Rabbit**	**Molecular Probe**	**A11061**	**IF**	**1:500**
RabbitAlexa488	**Goat**	**Molecular Probe**	**A11034**	**IF**	**1:500**
Mouse Alexa 568	**Goat**	**Thermo Fisher**	**A-11004**	**IF**	**1:1000**
Rabbit Alexa 488	**Goat**	**Thermo Fisher**	**A-11034**	**IF**	**1:1000**